# VARIATION AND POWER ISSUES IN VLSI CLOCK NETWORKS

A Dissertation

by

GANESH VENKATARAMAN

Submitted to the Office of Graduate Studies of
Texas A&M University
in partial fulfillment of the requirements for the degree of

DOCTOR OF PHILOSOPHY

May 2007

Major Subject: Computer Engineering

VARIATION AND POWER ISSUES IN VLSI CLOCK NETWORKS

A Dissertation

by

GANESH VENKATARAMAN

Submitted to the Office of Graduate Studies of
Texas A&M University
in partial fulfillment of the requirements for the degree of

DOCTOR OF PHILOSOPHY

Approved by:

| | |
|---|---|
| Chair of Committee, | Jiang Hu |
| Committee Members, | Sunil Khatri |
| | Vivek Sarin |
| | Weiping Shi |
| Head of Department, | Costas N. Georghiades |

May 2007

Major Subject: Computer Engineering

ABSTRACT

Variation and Power Issues in VLSI Clock Networks. (May 2007)

Ganesh Venkataraman, B. E. (Hons), Birla Institute of Technology and Science;

M. Sc. (Hons), Birla Institute of Technology and Science;

M. S., University of Iowa

Chair of Advisory Committee: Dr. Jiang Hu

Clock Distribution Network (CDN) is an important component of any synchronous logic circuit. The function of CDN is to deliver the clock signal to the clock sinks. Clock skew is defined as the difference in the arrival time of the clock signal at the clock sinks. Higher uncertainty in skew (due to PVT variations) degrades circuit performance by decreasing the maximum possible delay between any two sequential elements. Aggressive frequency scaling has also led to high power consumption especially in CDN. This dissertation addresses variation and power issues in the design of current and potential future CDN. The research detailed in this work presents algorithmic techniques for the following problems: (1) Variation tolerance in useful skew design, (2) Link insertion for buffered clock nets, (3) Methodology and algorithms for rotary clocking and (4) Clock mesh optimization for skew-power trade off.

For clock trees this dissertation presents techniques to integrate the different aspects of clock tree synthesis (skew scheduling, abstract topology and layout embedding) into one framework - tolerance to variations. This research addresses the issues involved in inserting cross-links in a buffered clock tree and proposes design criteria to avoid the risk of short-circuit current. Rotary clocking is a promising new clocking scheme that consists of unterminated rings formed by differential transmission lines. Rotary clocking achieves reduction in power dissipation clock skew. This dissertation addresses the issues in adopting current CAD methodology to rotary clocks. Alter-

native methodology and corresponding algorithmic techniques are detailed. Clock mesh is a popular form of CDN used in high performance systems. The problem of simultaneous sizing and placement of mesh buffers in a clock mesh is addressed. The algorithms presented remove the edges from the clock mesh to trade off skew tolerance for low power.

For clock trees as well as link insertion, our experiments indicate significant reduction in clock skew due to variations. For clock mesh, experimental results indicate 18.5% reduction in power with 1.3% delay penalty on a average. In summary, this dissertation details methodologies/algorithms that address two critical issues - variation and power dissipation in current and potential future CDN.

To my grandparents, parents and in special memory of my grandmom

ACKNOWLEDGMENTS

I must thank Dr. Jiang Hu for his guidance and support. He introduced me to Physical Design and served as a constant source of encouragement throughout my stay at Texas A&M.

I would like to thank the Semiconductor Research Corporation (SRC) for supporting my research. Many thanks to the Office of Graduate Studies at Texas A&M for granting the Graduate Merit Fellowship.

I have been fortunate enough to work with and learn from different professors and students throughout my doctoral studies. I would like to thank Dr. Sunil Khatri and Nikhil Jayakumar for helping me out with the link insertion work as well as some insightful discussions. I enjoyed working with Dr. Peng Li on developing driver models for fast simulation of clock mesh. Dr. Li's course introduced me to the exciting area of circuit simulation. I would like to thank Dr. Weiping Shi for teaching some very fine algorithmic concepts in VLSI CAD and for serving on my dissertation committee. I would like to thank Dr. Vivek Sarin for serving on my dissertation committee. The basic idea for clock mesh optimization was inspired from a lecture by Dr. Alex Sprintson. I would like to thank Dr. Sprintson for all the discussions. I am thankful to all my teachers - right from kindergarden for passing on their knowledge and wisdom.

I am deeply indebted to my uncle Dr. S. V. Ramakrishnan and aunt Mrs. Sita Ramakrishnan for their love and support. I would like to thank my grandparents for their incredible love. I would like to thank my parents, my brother and his wife for just about everything.

TABLE OF CONTENTS

LIST OF TABLES

LIST OF FIGURES

FIGURE                                                                    Page

CHAPTER I

INTRODUCTION

A.   Background and Motivation

Millions of transistors running in tandem have had a significant impact on our day-to-day life. Very Large Scale Integration (VLSI) is the process of creating Integrated Circuits (IC) by combining thousands of transistors on a single chip. The design, implementation, manufacturing and testing of VLSI circuits are done using automated computational techniques along with manual intervention as and when deemed necessary. The area of study devoted to developing algorithmic techniques and methodologies towards automating electronic design is commonly referred to as Electronic Design Automation (EDA).

For nearly three decades, the trend in the growth of IC design was dictated by an empirical observation also known as the Moore's Law. Moore's Law states that the number of transistors in a chip doubles every 18 months implying an exponential growth in transistor count. The operating frequency has so far been following the same trend. A key enabler of this rapid frequency scaling is constant reduction in minimum channel length of the CMOS transistor with every process generation. With every process generation also comes a new set of challenges for EDA. The function of EDA research is not just to solve the current problems but also identify the issues that may arise with future technologies. VLSI design involves multiple objectives like timing, power dissipation, area, manufacturing yield, testability etc. Very often these objectives might conflict with each other. A common example with conflicting objectives is power dissipation and circuit delay. Higher gate sizes could reduce circuit

_____

The journal model is IEEE Transactions on Automatic Control.

delay at the expense of higher power. EDA tools should also have the capability to trade off one objective for another and should allow the designer the flexibility to choose the desired trade off point.

Clock Distribution Network (CDN) is an integral part of any synchronous logic circuit. The function of CDN is to deliver the clock signal to the sequential elements. These elements are also referred to in literature as clock registers, flip-flops or clock sinks - all referring to the final destination of the clock signal. Clock skew between two clock sinks is defined as the difference between the arrival time of the clock signal at corresponding two clock sinks. Let $t_i$ denote the arrival time of the clock signal at sink $i$. In order to avoid a logic failure the skew between a register pair $(i, j)$ should be within the followings limits [1]:

$$t_{hold} - D_{min}^{ij} \leq t_i - t_j \leq T_{clock} - t_{setup} - D_{max}^{ij} \qquad (1.1)$$

In the above equation, $T_{clock}$, $t_{hold}$ and $t_{setup}$ denote the clock period, hold time and set up time respectively. $D_{max}^{ij}$ ($D_{min}^{ij}$) denotes the maximum (minimum) combinational delay between $i$ and $j$. Based on the assignment of arrival times, there are two types of CDN design: (1) Useful skew (also referred to as intentional skew) design, where clock skew is exploited to optimize design objectives such as wire length, clock frequency, tolerance of variations etc. (2) Zero Skew design, there CDN is constructed such that the arrival time of the clock signal at all the clock sinks is the same. For zero skew design, it is evident from Equation (1.1) that higher skew reduces the maximum delay possible between two sequential elements (implies a reduction in maximum circuit delay).

## 1. Impact of PVT Variations on Clock Skew

Process, voltage and temperature (often referred to as **PVT**) variations are becoming prominent factors that affect the design parameters of modern VLSI chips. Clock skew is a design parameter that is highly sensitive to PVT variations. On analyzing the impact of variations on the clock skew of a gigahertz microprocessor, it was observed that interconnect variations alone can cause up to 25% variation in clock skew [2]. Apart from interconnect, variation in clock skew can also occur from the following factors (1) power supply (2) clock buffer channel length and (3) sink load capacitance. Clock buffers are required to meet the constraints on signal slew and delay. The percentage of clock sinks in the total cell count keeps increasing with the successive process technologies. It has been projected that this number could rise to as much as **18.55%** in future technologies [3]. Higher number of clock sinks implies that we would need larger number of clock buffers to drive the clock net. This will mean larger variations in clock skew. Further, a 10% drop in power grid voltage (IR-drop) could cause 5-10% change in clock timing [4]. Further, the impact of IR-drop gets worst as voltage is scaled down. In summary, clock skew is susceptible to PVT variations and the effect is getting worst with technology scaling.

## 2. Power Dissipation in CDN

In CMOS, dynamic power is dissipated when the output switches value. The dynamic power dissipation is given by:

$$P_{dynamic} = \frac{1}{2} S_f V_{dd}^2 f_{clk} C_{load} \tag{1.2}$$

In the above equation $V_{dd}$ denotes the supply voltage, $f_{clk}$ the clock frequency, $C_{load}$ the load capacitance and $S_f$ the switching activity. For signal nets, $S_f$ is usually

between 0.10 and 0.20 [5]. The clock net switches every cycle. Hence, the switching activity equals 1 and this accounts for high power dissipation in the clock net. In high performance systems, the clock net could account for as much as 40% of the total power dissipation [6]. With the percentage of clock sinks increasing with every process generation [3], this figure could get higher. While power dissipation is of paramount importance in portable electronic devices, it has now become a significantly important design objective in high performance systems as well. Examples of such high performance systems include laptop computers (low power implies longer battery life) and server farms (commonly used in Internet search engines). In summary, the importance of power dissipation in VLSI design is becoming increasingly important. Since the clock net consumes a major portion of the total power dissipation, it is imperative to address this issue in EDA research.

## B.   Contributions

This dissertation deals with two keys in the design of modern CDN - variation and power dissipation. Figure (1) gives the overview of our contributions classified on the basis of different types of clock distributions. Our main contributions include (1) Variation tolerance in useful skew design (2) Link insertion for buffered clock nets, (3) Methodology and algorithms for rotary clocking and (4) Clock mesh optimization for skew-power trade off.

### 1.   Variation Tolerance in Useful Skew Design

Useful skew design consists of manipulating the clock skew in order to achieve the design objectives [7], such as high frequency and variation tolerance. We integrate all the above three steps namely - clock skew scheduling, abstract topology construction

Clock Distribution Network

| Tree: | Non Tree: | Rotary Clocking: |
|---|---|---|
| Variation tolerance in useful skew design | Extend Link Insertion for Buffered Networks Combinatorial algorithms for fast clock mesh optimization | Placement and scheduling methodology |
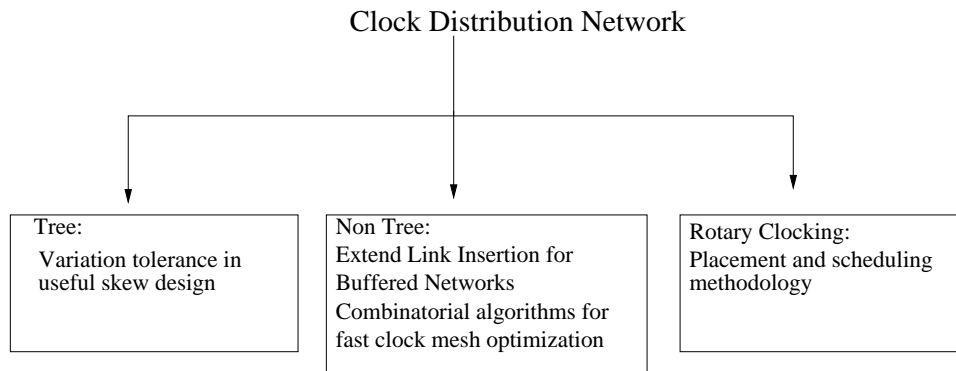
Fig. 1. Overview of the contributions.

and layout embedding in to one framework. The objective of the work is to minimize the maximum skew due to variations. In skew scheduling, an estimation of variations based on clock sink locations is employed to guide skew safety margin towards sink pairs which are more vulnerable to variations. Abstract topology is generated based on the estimated delay targets. In clock routing, an embedding technique is developed to minimize the maximum skew violation among all sink pairs **optimally**.

## 2.   Link Insertion for Buffered Clock Nets

Link insertion refers to the process of adding cross-links to a clock tree thereby converting it into a non-tree. The primary purpose of link insertion is to improve the tolerance of the tree towards variations in clock skew. Link insertion has been shown to provide an effective trade off between skew reduction and increase in wire length. Previous works on link insertion focused on unbuffered clock networks [8, 9]. In reality, buffers are required to meet constraints on signal slew and delay. The main contributions of the work include:

- Link insertion in a buffered network may result in multiple drivers for a subnet.

A design criterion for avoiding short circuit risk in a multi-driver net is proposed.

- Skew tuning is used to synthesize a clock tree with low nominal skew under a higher order delay model. The effect of link insertion depends on a well-designed buffered clock tree. The proposed technique can decrease nominal clock skew considerably and therefore enhances the effectiveness of link insertion.

- A complete methodology of link based buffered clock network under accurate gate and wire delay models is proposed. This methodology utilizes the buffered clock tree construction techniques which are friendly to link insertion.

- The proposed method is validated with HSPICE based Monte Carlo simulations considering spatially correlated power supply variations, buffer and wire process variations.

## 3. Methodology and Algorithms for Rotary Clocking

In order to solve the power and the variation problem more effectively, several novel clocking technologies have been developed. Among them, rotary traveling wave clock is a promising approach [10]. The basic component of a rotary clock is a pair of cross-connected differential transmission line circles, namely a rotary clock ring. A clock signal propagates along the ring without termination so that the energy can be recirculated and the charging/discharging power dissipation is greatly reduced.

There is one technical hurdle that prevents wide applications of the rotary clock: the clock signal has different phases at different locations on the rotary clock ring. If zero skew design is insisted, the usage of rotary clocks would be very restrictive. Hence, non-zero intentional skew design is a better approach to fully utilize the rotary clock. Unlike the intentional skew design in the conventional clocking technology where no restrictions are imposed on the flip-flop locations, the skew at each flip-flop

has to be matched with a specific location at the rotary clock ring. This requirement forms a difficult chicken-and-egg problem: the flip-flop placement depends on skew optimization while it is well known that skew optimization depends on flip-flop locations. This is quite different from traditional intentional skew designs where the placement does not depend on skew optimization.

We make the following contributions:

- A relaxation technique based on flexible tapping is suggested to break the loop in the chicken-and-egg problem.

- An integrated placement and skew optimization methodology is proposed to facilitate the application of rotary clocking. This methodology has the advantage that traditional placement methods can be employed directly without any change.

- A min-cost network flow algorithm is found to assign flip-flops to the rotary clock rings so that the movement of flip-flops has the least disturbance to traditional placement.

- A pseudo net technique is introduced to guide flip-flops toward their preferred locations without intrusive disturbance to traditional placement.

- A cost driven skew optimization formulation is developed to reduce the connection cost between flip-flops and their corresponding rotary clock rings.

Our techniques can be easily augmented with existing CAD tools/flow thereby making rotary clocks usable for practical designs.

## 4. Combinatorial Algorithms for Fast Clock Mesh Optimization

Clock mesh is a popular form of CDN used in high performance systems [11, 12, 13]. Mesh has a high tolerance to variations. The tolerance comes from the redundancy created by the multiple paths between the clock source and the sinks. However, such a high tolerance comes at an expense of increased resource consumption - namely high wire length and power dissipation. Mesh is usually driven by a top-level tree with buffers at the leaves of the this tree - henceforth referred to as **mesh buffers**. Previous works on clock mesh do not address the issue of where to place the mesh buffers in the clock mesh. It is also not clear if there is a scope to use buffers of different size. We address the issue of mesh buffer sizing as well as their placement in the mesh. We then remove the edges in the mesh to trade off the skew tolerance for lower power dissipation. Our contributions include:

- We propose a set-cover based algorithm for finding the mesh buffer locations and their sizes. Our algorithm works fast on a discrete library of buffer sizes. We show that such a buffer placement and sizing yields better results compared to uniform sizing.

- We formulate the mesh reduction problem by using survivable network theory. We present heuristics for solving the formulation efficiently.

- Our techniques allow the designer to trade off between skew and power dissipation. In fact, the formulation presented is flexible enough to allow a high range of trade off (that is either a high skew- low power design or a low skew - high power design or anywhere in between).

- Our algorithms run very fast. It can process test cases with over a thousand sinks within a few seconds. Such a high speed helps the designer to run the same

algorithm several times with different parameter values that produce different solutions in the power delay curve.

## C.  Organization

The remainder of this dissertation is organized as follows.  Chapter II deals with variation tolerance in useful skew design. We detail some of the problems encountered while inserting links in buffered clock nets in Chapter III. We then proceed to describe our procedure for clock tree generation as well as link insertion. Chapter IV details the issues involved in adopting the current CAD methodologies for rotary clocking. We then propose our flow and corresponding algorithms.  Chapter V details our work on clock mesh optimization. We present fast algorithms for simultaneous mesh buffer placement and sizing.  This chapter also presents mesh reduction techniques. Chapter VI details our conclusions.

CHAPTER II

VARIATION TOLERANCE IN USEFUL SKEW DESIGN

This chapter details our techniques that improve variation tolerance in useful skew design. The objective of the work is to minimize the maximum deviation of clock skew from the allowed limits.

A.   Preliminaries

The following notations/conventions will be followed in this chapter:

- Clock sinks, registers and flip-flops refer to sequential elements unless otherwise specified.

- Two clock sinks are said to be **sequentially adjacent** if they have only combinational logic between them.

- $S = \{s_1, s_2, ...s_n\}$ denotes the set of clock sinks.

- $C_i$ denotes the sink load capacitance.

- For each sink $i$, $t_i$ denotes the signal arrival time.

- $T_{clock}$, $t_{hold}$ and $t_{setup}$ denote the clock period, hold time and set up time respectively.

- $D_{max}^{ij}$ ($D_{min}^{ij}$) denotes the maximum (minimum) combinational delay between sinks $i$ and $j$.

- In order to avoid a logic failure the skew between a register pair $(i, j)$ should be within the followings limits [1]:

$$t_{hold} - D_{min}^{ij} \leq t_i - t_j \leq T_{clock} - t_{setup} - D_{max}^{ij} \tag{2.1}$$

- $t^l(i,j) = t_{hold} - D_{min}$ and $t^u(i,j) = T - t_{setup} - D_{max}$ form the lower and upper skew permissible range respectively.

- $w$ denotes the wire width.

- The capacitance of an interconnect of length $l$ is given by $c \cdot l \cdot w$, where $c$ denotes the capacitance per unit area.

- The resistance of an interconnect of length $l$ is given by $r \cdot \frac{l}{w}$ where $r$ denotes the sheet resistance.

- We assume the wire width and sink load variations follow normal distributions and the variation is approximately bounded by the $3\sigma$ value represented by $W_l \leq w \leq W_u$ and $C_i^l \leq C_i \leq C_i^u$.

- The **skew violation** due to variations is defined as:

$$t^{vio}(i,j) = \max(t^l(i,j) - t_{ij}, t_{ij} - t^u(i,j)) \qquad (2.2)$$

- $T(v_i)$ denotes the subtree with root node $v_i$.

- $ms(v_i)$ denotes the merging segment at node $v_i$.

- As in the previous works [7, 14], we employ the Elmore delay model [15, 16].

B. Previous Work

Zero Skew Tree **(ZST)** refers to a clock tree where the arrival time of the clock signal at all the sinks is the same. The input to ZST construction is a set of clock sinks, their positions (or co-ordinates) and the load capacitances at each sink. The output is a tree connecting all the sinks to the source that minimizes the wire length subject

to the constraint that the arrival time of the clock signal at **all** the clock sinks is the same.

Most published works on clock tree construction follow the framework laid down by the Deferred Merge Embedding (DME) algorithm [17]. DME consists of two phases (a) Bottom-up phase and (b) Top down phase. The bottom-up phase is recursive and at any given point it operates on a set of subtrees. Initially, the set of subtrees is the set of clock sinks. Subtrees are merged in such a manner that all clock sinks that are part of the merged subtree have the same signal arrival time [18]. In other words, while merging two subtrees (to form one subtree), the merging point is chosen in such a manner that zero skew is maintained. The main aspect of DME lies in the following key observation. The merging point to maintain zero skew is not a single point but a locus of points in the 2-dimensional plane - also referred to as the **merging segment**. Figure (2) illustrates the concept of merging segments. In the figure $v_i$ and $v_j$ denote the subtrees to be merged. In-order to meet the zero skew constraints the distance from the root of $v_i$ ($v_j$) to the merged subtree should be $ev_i$ ($ev_j$). The distances can be computed using the technique detailed in [18]. Distance refers to Manhattan distance unless otherwise specified. It was shown in [17] that the locus of the points that satisfy the distance constraint corresponds to a Manhattan arc (shown in dotted lines in Figure (2)). The bottom-up phase of DME proceeds in this fashion to compute a bunch of merging segments. After completion of the bottom-up phase, we are left with one subtree. The top-down phase chooses the actual location of the merging points in order to minimize the wire length.

In reality the clock skew need not be zero across all the sink pairs. Clock skew for every pair of registers need to be within the bounds dictated by Equation (2.1). The idea of exploiting the skew constraints as indicated in Equation (2.1) is referred to as Useful Skew Tree **(UST)** design. Clock tree construction for useful skew design
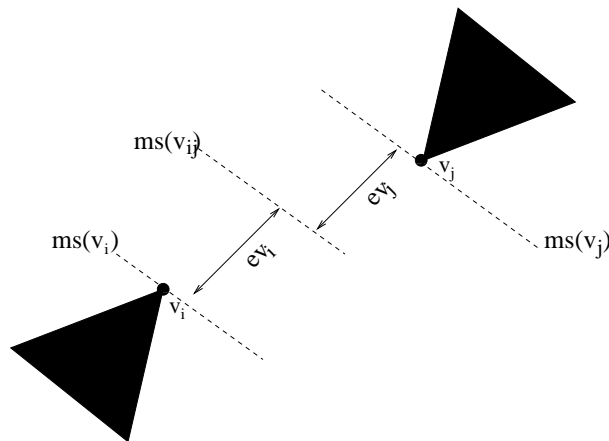
Fig. 2. Merging and embedding of subtrees.

usually follows three stages:

1. Clock skew scheduling - determines the relative clock signal delay for each clock sink (also known as the delay targets), the objective is usually to minimize clock period.

2. Abstract topology generation - determines the merging order of the clock sinks in the clock tree.

3. Layout embedding - determines the location of the merging point such that the skew constraints are satisfied.

Clock skew scheduling can be stated as a linear programming (LP) problem [1]. The objective could be to maximize the operating clock frequency or to increase the tolerance to variations. The LP could then be solved using standard LP-solvers or using combinatorial techniques [19].

Since DME assumes the abstract topology of the tree is given (that is, part of the input), it is important to employ a good topology generation scheme that suits

the target objective. The usual objective in topology generation is to minimize the total wire length. An effective way to choose the merging order is to use clustering and Delaunay triangulation at the same time [20]. An uncertainty driven abstract tree construction algorithm was proposed in [21]. The authors use the observation that the variations in clock skew (between two clock sinks) is caused only due to timing variations in the uncommon region between the two corresponding clock sinks in the clock tree. Hence the proposed technique merges clock sinks based solely on their skew permissible range. However, this scheme does not consider the physical distance and could end up merging sinks that are far apart earlier in the tree thereby increasing the wire length. An abstract topology algorithm for useful clock skew was presented in [22]. Each sink is assigned a delay-target - which can be obtained from skew scheduling. The delay targets are updated when a new subtree is created upon merging two subtrees whose delay targets are known. The first subtree is chosen to be the one with the maximum delay target. The second subtree is chosen on the basis of distance. Hence the merging scheme is aware of both skew scheduling and distance. However such a scheme assumes that skew schedule (or delay target of sink nodes) is part of the input. In the work presented in UST/DME [7], the clock routing is integrated with incremental skew scheduling such that further wire length reduction is obtained compared with DME. However, process variations are not considered in UST/DME. Process variation aware layout embedding was considered in [14]. The authors employ a heuristic to find a critical pair among all possible pairs in the merged subtree. The authors then try to optimize the layout embedding scheme for this chosen pair. Since the optimization is done for only one pair, it is possible that that other sink pairs might have a lower safety margin in their skew.

C.   Problem Statement

*Given a set of clock sinks $S = \{s_1, s_2, ...s_n\}$, and a set of skew constraints as shown in Equation (2.1), find the clock arrival time assignment $t_i$ for each clock element $s_i$ and construct a clock tree such that the maximum skew violation among all pairs of clock sinks is minimized while wire width varies between $W_u$ and $W_l$ and load capacitance $C_i$ of each sink $s_i$ varies between $C_i^l$ and $C_i^u$.*

D.   Algorithm

1.   Algorithm Overview

Our algorithm consists of two major parts: (1) variation aware skew scheduling and (2) variation aware clock routing. The algorithm overview is provided in Figure (3).

In the variation aware skew scheduling, an estimated skew variation between each pair of sequentially adjacent registers is computed based on their locations. Then, a linear programming based skew scheduling algorithm is performed to maximize the relative skew safety margin according to the estimated skew variations. The delay target to each register is obtained after skew scheduling.

The variation aware clock routing is a procedure of interleaving abstract tree generation with layout embedding. The abstract tree generation or the merging scheme is similar to [22] and consists of two steps: (1) finding a sink node $v_r$ (which is a part of the subtree say $T(v_i)$) with the maximum delay target and (2) finding the other sink node $v_l$ (which is a part of subtree say $T(v_j)$) to be merged with $T(v_i)$ such that the merging cost is minimized. The merging cost will be defined later. The layout embedding is based on DME with consideration on process variations. The merging segment between subtrees $T(v_i)$ and $T(v_j)$ is found such that the maximum skew violation between sinks of two subtrees is minimized.

Algorithm Overview

Clock Scheduling and Routing

Input : clock sinks, initial skew permissible range

Output : clock tree routing

begin

1. Estimate skew guarding band for each pair of sequentially adjacent registers

2. Find delay target to each register such that variation aware safety

   margin is maximized

3. Variation aware clock routing, Subtree set $B = \{s_1, s_2, ..., s_n\}$

   While ( $|B| > 1$ )

       3.1 Abstract tree generation

           3.1.1 Select sink $v_r$ (part of subtree $T(v_i)$) with max delay target

           3.1.2 Select another sink $v_l$ (part of subtree $T(v_j)$)to be merged such

               that the merging wire length is minimized

       3.2 Variation aware embedding

           Find merging segment for $T(v_i)$ and $T(v_j)$ such that $t^{vio}(i, j)$ between

           each pair $m \in T(v_i)$and $n \in T(v_j)$ is minimized

       3.3 $B \leftarrow B - (T_l, T_r) +$ Newly formed subtree

   end while

Fig. 3. Scheduling and routing algorithm.

## 2. Process Variation Aware Skew Scheduling

In skew scheduling, delay target $t_i$ to each register $i$ is determined while the permissible range as defined by Equation (2.1) is satisfied. In order to improve tolerance to process variations, the skew safety margin $\min(t^u(i,j) - t_{ij}, t_{ij} - t^l(i,j))$ needs to be maximized for each pair of sequentially adjacent registers. Since the distance between each pair of registers may be different from each other, the skew variation for each pair is usually different from each other as well. Therefore, different amount of safety margin should be allocated for different register pairs. The objective of our skew scheduling scheme is to maximize skew safety margin with consideration of skew variation between registers. If the estimated skew variation between register $i$ and $j$ is $\delta_{ij}$, we formulate the scheduling problem as:

$$\text{Maximize} \qquad M \qquad\qquad (2.3)$$

$$\forall \text{ seq adj reg } i \text{ and } j$$

$$M \le t^u(i,j) - \delta_{ij} - (t_i - t_j)$$

$$M \le (t_i - t_j) - t^l(i,j) - \delta_{ij}$$

where $M$ is the shared safety margin for each pair. This formulation may allocate safety margins according to anticipated variation effect instead of uniform allocation in previous works [1, 23, 24]. This linear programming problem can be solved by the binary search method introduced in [19].

The estimated skew variation is obtained based on distance between registers since the clock routing information is not available in the scheduling stage. For two registers $i$ and $j$, we assume they are merged at the middle point between them and use the skew variation from this merging as an estimation. A wire segment of length $l$ driving a load of $C_l$ has delay of $\frac{1}{2}rcl^2 + \frac{rl}{w}C_L$. If wire width $w$ varies around nominal

value $w_0$ with bound of $w_0 \pm dw$ and sink load varies as $C_{Li} = C_{0Li} \pm dC_{Li}$, the skew variation between $i$ and $j$ is estimated to be:

$$\delta_{ij} = \frac{D_{ij}r}{2w_0}(dC_{Li} + \frac{C_{Li} \cdot dw}{w_0} + dC_{Lj} + \frac{C_{Lj} \cdot dw}{w_0}) \tag{2.4}$$

where $D_{ij}$ is the Manhattan distance between register $i$ and $j$. Even though this estimation is an approximation, it reflects the trend that variability may grow with distance.

### 3.  Process Variation Aware Layout Embedding

In this section, we detail a layout embedding scheme that aims to minimize the maximum violation in skew due to process variation. Process variation aware embedding was handled in [14], where a heuristic was used to identify a single critical pair and the layout embedding focused on this pair alone. In our work, we propose a formulation that considers the effect due to variation in all pairs.

Consider two subtrees $T(v_i)$ and $T(v_j)$ to be merged. In our approach, we shall show that there exists a locus of points that has fixed distances from merging segments $ms(v_i)$ and $ms(v_j)$ such that it minimizes the maximum skew violation. Maximum skew violation is defined as the maximum deviation of the skew from its allowed bounds among all sequentially adjacent register pairs. Let $T_{max}^{vio}$ denote the maximum skew violation. Then:

$$T_{max}^{vio} = \max_{(i,j)}(t^l(i,j) - t_{ij}, t_{ij} - t^u(i,j)) \tag{2.5}$$

Ideally, we would like $T_{max}^{vio}$ to be negative implying that there is no violation. We first formally state the problem that is addressed in this section.

**Process variation aware layout embedding**

*Given two subtrees $T(v_i)$ and $T(v_j)$ to be merged, find a parent merging segment*

$ms(v_{ij})$ *such that the maximum skew violation among all sequentially adjacent pairs* $(s_r, s_l)$ *where* $s_r \in T(v_i)$ *and* $s_l \in T(v_j)$ *is minimized.*

The above problem can also be formulated mathematically as described below. For $s_r \in T(v_i)$ and $s_l \in T(v_j)$, let $\overline{t_{rl}}(e_{v_i}, e_{v_j})$ ($\underline{t_{rl}}(e_{v_i}, e_{v_j})$) denote the maximum (minimum) skew between $s_r$ and $s_l$ due to process variation. Let $t_{rl}$ denote the nominal skew value. We intend to minimize the maximum skew violation, or equivalently maximize the minimum difference between the skew bounds and the worst case skew among all pairs. This is similar to the scheduling described in Equation (2.3) and can be written as:

$$\text{Maximize } S_{ij} \qquad\qquad (2.6)$$

$$\forall\ r \in T(v_i) \text{ and } l \in T(v_j)$$

$$S_{ij} \leq t^u(r,l) - \overline{t_{rl}}(e_{v_i}, e_{v_j})$$

$$S_{ij} \leq \underline{t_{rl}}(e_{v_i}, e_{v_j}) - t^l(r,l)$$

where $S_{ij}$ is a variable similar to the safety margin in skew scheduling. Maximizing $S_{ij}$ is equivalent to minimizing skew violation.

The procedure to evaluate $\overline{t_{rl}}(e_{v_i}, e_{v_j})$ and $\underline{t_{rl}}(e_{v_i}, e_{v_j})$ under variation in wire-width and load capacitances was detailed in [14]. We shall state it in brief and show how formulation (2.6) can be transformed into a mathematical programming problem with quadratic constraints. We also outline a technique which can be used to solve this problem. Though we concentrate on wire-width and load capacitance variations, the formulation given in (2.6) is generic and can be easily modified to take care of other variations as well.

$(\underline{t_r}, t_r, \overline{t_r})$ denote the minimum, nominal and maximum delays from $s_r$ (which is part of the subtree $T(v_i)$) to the node $v_i$. $(C_i^l, C_i, C_i^u)$ represent the minimum, nom-

inal and maximum downstream capacitances at node $v_i$ respectively. Let $\alpha_i^l(\alpha_i^u) = r\frac{C_i^l}{W_u}(r\frac{C_i^u}{W_l})$ and $\phi = \frac{1}{2}rc$. Then:

$$\overline{t_{rl}}(e_{v_i}, e_{v_j}) = (\overline{t_r} + \phi e_{v_i}^2 + \alpha_i^u e_{v_i}) - (\underline{t_l} + \phi e_{v_j}^2 + \alpha_j^l e_{v_j}) \qquad (2.7)$$

$W_u$ and $W_l$ denote the bounds on the wire width. Interested reader may refer to [14] for detailed derivation of the these equations.

Similarly $\underline{t_{rl}}(e_{v_i}, e_{v_j})$ may be written as:

$$\underline{t_{rl}}(e_{v_i}, e_{v_j}) = (\underline{t_r} + \phi e_{v_i}^2 + \alpha_i^l e_{v_i}) - (\overline{t_l} + \phi e_{v_j}^2 + \alpha_j^u e_{v_j}) \qquad (2.8)$$

We can transform the formulation (2.6) into a mathematical programming problem using equations (2.7) and (2.8).

$$\text{Maximize } S_{ij} \qquad (2.9)$$

$$\forall\ r \in T(v_i) \text{ and } l \in T(v_j)$$

$$S_{ij} \leq (t^u(r, l) - \overline{t_r} + \underline{t_l}) - \phi(e_{v_i}^2 - e_{v_j}^2) - (\alpha_i^u e_{v_i} - \alpha_j^l e_{v_j})$$

$$S_{ij} \leq (-t^l(r, l) - \overline{t_l} + \underline{t_r}) + \phi(e_{v_i}^2 - e_{v_j}^2) + (\alpha_i^l e_{v_i} - \alpha_j^u e_{v_j})$$

$$e_{v_i}, e_{v_j} \geq 0\ \ e_{v_i} + e_{v_j} \geq D_{ij}$$

The above formulation is quite different from the work in [14] where a single pair of critical sinks were identified. After this, embedding was done in such a way that the center of the worst case skew matches with the center of the permissible range. However, this is a heuristic and there could be other pairs (other than the critical one) which could face a significant deviation in skew due to process variations. Formulation (2.6) attempts to overcome this difficulty. The parent merging segment cannot exist if $(e_{v_i} + e_{v_j} < D_{ij})$ and the final constraint takes care of that. The formulation appears to be a difficult one to solve because of the presence of quadratic constraints.

But, we can consider two separate cases: case 1 does not require any wire snaking and case 2 requires wire snaking. In each of these cases, the formulation can be transformed in to another one with linear constraints. The method to identify the need for wire snaking has been presented in [14].

**Case 1: No wire snaking**

In this case, $e_{v_i} + e_{v_j} = D_{ij}$. Define the following parameters:

$$m_1(r, l) = (t^u(r, l) - \overline{t_r} + \underline{t_l}) + \phi D_{ij}^2 + \alpha_j^l D_{ij} \tag{2.10}$$

$$m_2(r, l) = (-t^l(r, l) - \overline{t_l} + \underline{t_r}) - \phi D_{ij}^2 - \alpha_j^u D_{ij}$$

$$k_1 = 2\phi D_{ij} + \alpha_i^u + \alpha_j^l, \quad k_2 = 2\phi D_{ij} + \alpha_j^u + \alpha_i^l$$

With no snaking formulation (2.9) gets modified in to the following linear programming problem with just one variable:

$$\text{Maximize } S_{ij} \tag{2.11}$$

$$\forall \, r \in T(v_i) \text{ and } l \in T(v_j), \quad S_{ij} \leq m_1(r, l) - k_1 e_{v_i}$$

$$S_{ij} \leq m_2(r, l) + k_2 e_{v_i}, \quad e_{v_i} \geq 0$$

Notice that the constraints in (2.11) represent straight lines with a positive slope of $k_2$ or the negative slope of $-k_1$. For the same pair of subtrees $T(v_i)$ and $T(v_j)$, $k_1$ and $k_2$ are the same for all $(r, l)$. We have two sets of lines with lines in the same set parallel to one another. Figure (4) gives a plot of the lines when there are two such pairs. The upper half of the figure gives 4 straight lines that represent the 4 inequality constraints (in (2.11) ) corresponding to the 2 pairs. The lower half plots the values of $S_{ij}$ as $e_{v_i}$ is increased. Let $m_1(r_1, l_1) = \min_{r \in T(v_i), l \in T(v_j)} m_1(r, l)$ and $m_2(r_2, l_2) = \min_{r \in T(v_i), l \in T(v_j)} m_2(r, l)$.

**Lemma 1**

If no snaking is required, that is $0 \leq e_{v_i}, e_{v_j} \leq D_{ij}$, then the optimal solution to (2.11) exists at a point

$$e_{v_i} = \frac{m_1(r_1, l_1) - m_2(r_2, l_2)}{k_1 + k_2} \tag{2.12}$$

The proof is Lemma 1 is straightforward and Figure (3) gives the geometric intuition behind the proof.

**Case 2: With wire snaking**

Wire snaking could mean either $(e_{v_i} = 0, e_{v_j} > D_{ij})$ or $(e_{v_i} = 0, e_{v_j} > D_{ij})$. We discuss the latter and the equations can be modified to fit the former. Let $m_1'(r, l) = (t^u(r, l) - \overline{t_r} + \underline{t_l})$ and $m_2'(r, l) = (-t^l(r, l) - \overline{t_l} + \underline{t_r})$. When we substitute $e_{v_i} = 0$ in formulation (2.9) we get:

$$\text{Maximize } S_{ij} \tag{2.13}$$

$$\forall \, r \in T(v_i) \text{ and } l \in T(v_j)$$

$$S_{ij} \leq m_1'(r, l) + \phi e_{v_j}^2 + \alpha_j^l e_{v_j}$$

$$S_{ij} \leq m_2'(r, l) - \phi e_{v_j}^2 - \alpha_j^u e_{v_j}, \quad e_{v_j} \geq 0$$

The optimal solution for (2.13) is obtained in a manner similar to that discussed for case 1. Here, we have non-linear terms. But still the coefficients of $e_{v_j}$ and $e_{v_j}^2$ are the same for all $(r, l)$. Let $m_1'(r_1, l_1) = \min_{r \in T(v_i), l \in T(v_j)} m_1'(r, l)$ and $m_2'(r_2, l_2) = \min_{r \in T(v_i), l \in T(v_j)} m_2'(r, l)$.

**Lemma 2**

If wire snaking is required with $e_{v_i} = 0$ and $e_{v_j} > D_{ij}$, then the optimal solution to (2.13) exists at a point $e_{v_j}$ that satisfies the following equation:

$$m_1'(r_1, l_1) + \phi e_{v_j}^2 + \alpha_j^l e_{v_j} = m_2'(r_2, l_2) - \phi e_{v_j}^2 - \alpha_j^u e_{v_j} \tag{2.14}$$
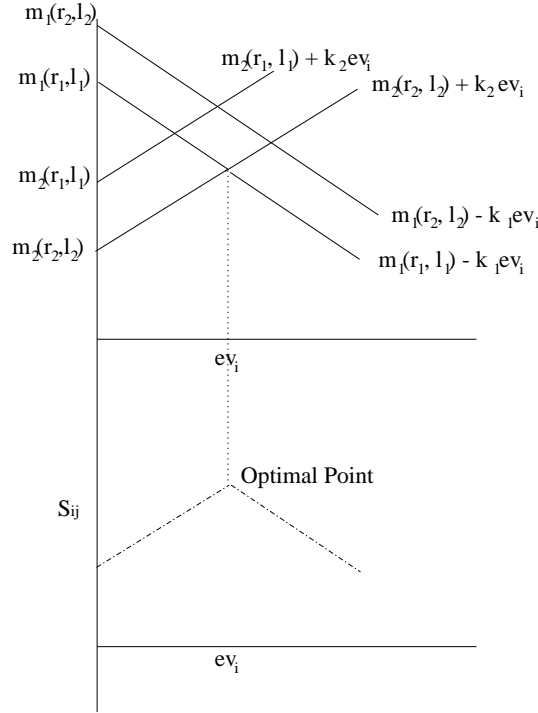
Fig. 4. Plot of $S_{ij}$ with two pairs.

## 4.   Alternative Layout Embedding

An alternative embedding procedure was also performed to make a comparison with our proposed scheme. This method closely follows [14] with a key difference. In [14], one critical pair was selected using a weighted function that considers both the physical distance as well as the permissible range. Here we consider the feasible skew range (FSR) [7] instead of the permissible range. The FSR matrix is updated after every merge operation. After such an update, it is possible that the feasible skew range of two sinks (say $s_r$ and $s_l$) gets reduced. Interested reader may refer to [7] for a detailed description of the FSR matrix and the process used to update it after every merge. In such a scenario, we reduce the range by an additional factor ($\delta_{rl}$) whose value equals the difference between the maximum and the nominal skew multiplied

by a scaling factor. This way, we have an incremental scheduling scheme that reflects the effect due to process variation.

## 5. Abstract Tree Generation

We first select a sink node ($s_a$ in a subtree rooted at $v_i$) which has the maximum delay target. The second node is selected based on basis of expected wire length added. Consider a sink node $s_b$ in a subtree rooted at ($v_j$). We compute the values of $e_{v_i}$ and $e_{v_j}$ by the following procedure. To compute the actual values of $e_{v_i}$ and $e_{v_j}$, we first need to find two sink pairs $(r_1, l_1)$ and $(r_2, l_2)$ such that $m_1(r_1, l_1) = \min_{r \in T(v_i), l \in T(v_j)} m_1(r, l)$ and $m_2(r_2, l_2) = \min_{r \in T(v_i), l \in T(v_j)} m_2(r, l)$. This could be prohibitively expensive for all pairs. So we use the heuristic where we assign $(r_1, l_1) = (r_2, l_2) = (a, b)$. Then by using the procedure detailed earlier, we identify the need for snaking and use equation (2.12) or (2.14) to compute $e_{v_i}$ and $e_{v_j}$. This serves as the merging cost. We claim that such a heuristic performs better and have experimental results to support the claim. This procedure will be referred to as *embedding aware abstract topology construction.*

## 6. Algorithm Complexity

The complexity of the process variation aware scheduling is $O(nm)$ where $n$ is the number of sinks and $m$ is the number of constraints for the linear programming formulation. The complexity of each embedding is $O(n)$ and the total run time for $O(n)$ embeddings is $O(n^2)$. Even though $m = O(n^2)$ in theory, in practice $m = O(n)$. Therefore, the overall complexity of our algorithm is $O(n^2)$.

E.   Experimental Results

The proposed procedure was tested on five benchmark circuits [18]. The values of the technology parameters used were obtained from [14]. The benchmark circuits do not contain the timing information (permissible range for each sink pair). So, we generated the permissible ranges randomly such that for every $(s_r, s_l)$, $t^l(r, l) < 0 < t^u(r, l)$. The permissible ranges were not symmetric but chosen such that $||t^u(r, l)| - |t^l(r, l)|| < 100ps$, $t^l(r, l) \in (-600ps, -100ps)$ and $t^u(r, l) \in (100ps, 600ps)$. The code was written in C and run on a Sun Solaris Ultra Sparc machine with 2 GB RAM.

We ran our experiments for five methods (based on scheduling, topology and embedding) denoted as:

- BASE CASE: No scheduling, topology based on distance, embedding follows [14]

- SP-DISTANCE: Process variation aware scheduling, topology based on distance, embedding follows [14]

- MP-DISTANCE: Process variation aware scheduling, topology based on distance, the new embedding scheme

- SP-eAWARE: Process variation aware scheduling and topology, embedding follows [14]

- MP-eAWARE: Process variation aware scheduling and topology, the new embedding scheme

In the above mentioned methods, BASE CASE is almost similar to [14] and MP-eAWARE represents our complete solution proposed. Experiments were run on the remaining three methods to show the effect of each individual technique, thereby providing a better insight. Monte Carlo simulations (1000 runs) were done for all

Table I. Results for the base case.

| Case | #Sinks | BASE CASE | | | |
|---:|---:|---:|---:|---:|---:|
| | | WL | #Vio | Max Vio | CPU |
| r1 | 267 | 1.97 | 0.21 | 3.43 | 00:01 |
| r2 | 598 | 3.85 | 18.60 | 69.91 | 00:06 |
| r3 | 862 | 4.59 | 33.37 | 88.52 | 00:13 |
| r4 | 1903 | 9.53 | 553.39 | 573.64 | 00:51 |
| r5 | 3101 | 14.39 | 1523.30 | 1392.39 | 02:31 |

five methods. In each run, the wire width and load capacitance were chosen at random from a uniform distribution with mean being the nominal value and standard deviation set such that $3\sigma$ corresponds to 10% deviation from the nominal value. Table (I) shows the results for BASE CASE, Table (II) for SP-DISTANCE and MP-DISTANCE, Table (III) for SP-eAWARE and MP-eAWARE. The sub columns represent wire length (WL) (in 1e+6$\mu$m), Number of violations (#Vio), average maximum violation in $ps$ (Max Vio) CPU (in min:sec) and Improvement (of maximum violation in percentage compared to the base).

As it is evident from the Table (III) there is a significant difference in the maximum skew violation between our proposed scheme and the base case. Moreover (MP-DISTANCE, MP-eAWARE) perform better than (SP-DISTANCE, SP-eAWARE) highlighting the effectiveness of our embedding technique. Our primary focus is to reduce the maximum skew violation and not number of violations since the former has a greater impact on the choice of the clock frequency. For example consider two scenarios: case (a) 50 violations with a maximum violation of 25 $ps$ and case (b) 1 violation of 50 $ps$. Case (a) could be handled by slowing the clock by 25 $ps$ whereas

case (b) would require a reduction of 50 $ps$ in clock speed. Nevertheless, proposed technique results in a significant gain in the number of violations as well.

Table II. Single pair and multiple pair embedding schemes - when abstract topology is distance based.

| Case | SP-DISTANCE | | | | | MP-DISTANCE | | | | |
|---|---|---|---|---|---|---|---|---|---|---|
| | WL | #Vio | Max Vio | CPU | Imp(%) | WL | #Vio | Max Vio | CPU | Imp(%) |
| r1 | 1.87 | 0.01 | 0.07 | 00:03 | 98.11 | 1.83 | 0.00 | 0.00 | 00:01 | 99.85 |
| r2 | 3.84 | 6.98 | 42.57 | 00:16 | 39.11 | 3.80 | 2.93 | 17.80 | 00:06 | 74.54 |
| r3 | 4.39 | 27.55 | 93.87 | 00:40 | -6.04 | 4.37 | 15.95 | 58.73 | 00:14 | 33.65 |
| r4 | 9.25 | 516.73 | 544.63 | 02:40 | 5.07 | 9.33 | 521.49 | 488.19 | 00:56 | 14.90 |
| r5 | 14.37 | 1491.21 | 1383.35 | 05:09 | 0.65 | 14.44 | 1474.21 | 1251.36 | 02:20 | 10.13 |

Table III. Single pair and multiple pair embedding schemes - when abstract topology is embedding aware.

| Case | SP-eAWARE | | | | | MP-eAWARE | | | | |
|---|---|---|---|---|---|---|---|---|---|---|
| | WL | #Vio | Max Vio | CPU | Imp(%) | WL | #Vio | Max Vio | CPU | Imp(%) |
| r1 | 1.81 | 0.02 | 0.16 | 00:03 | 95.46 | 1.81 | 0.00 | 0.00 | 00:01 | 100.00 |
| r2 | 3.74 | 2.01 | 20.14 | 00:14 | 71.19 | 3.72 | 0.75 | 7.37 | 00:06 | 89.46 |
| r3 | 4.38 | 30.99 | 85.72 | 00:39 | 3.16 | 4.38 | 16.27 | 69.19 | 00:14 | 21.84 |
| r4 | 9.25 | 496.53 | 522.21 | 02:31 | 8.97 | 9.21 | 457.41 | 483.28 | 00:55 | 15.75 |
| r5 | 13.96 | 1422.69 | 1228.44 | 04:57 | 11.77 | 14.17 | 1337.42 | 1128.81 | 02:21 | 18.93 |

CHAPTER III

LINK INSERTION IN BUFFERED CLOCK NETS

Link insertion consists of adding cross-links to an existing clock tree, thereby converting it in to a non-tree. The primary objective of link insertion is to increase the tolerance of the clock network to PVT variations. In this chapter, we address the issues involved in inserting links in a buffered clock network. We analyze the short-circuit risk involved in inserting cross links in a buffered tree. Based on this analysis, we propose a design criteria to avoid the risk. Link insertion assumes a zero skew tree as input. We detail a skew tuning technique that produces low skew trees. In the experimental section, we compare the variation and power results of our approach with clock trees as well as clock mesh (a popular form of non-tree based clock distribution).

A.  Preliminaries

The following notations/conventions will be followed in this chapter:

- $S = \{s_1, s_2, ...s_n\}$ denotes the set of clock sinks.

- The capacitance of an interconnect of length $l$ is given by $c \cdot l$, where $c$ denotes the capacitance per unit length.

- The resistance of an interconnect of length $l$ is given by $r \cdot l$ where $r$ denotes the resistance per unit length.

- For initial tree construction, we use linear delay model for the buffers. The delay of a buffer is given by:

$$t_{buf} = r_b C_{load} + t_b \tag{3.1}$$

In the above equation $r_b$ denotes the resistance and $t_b$ the intrinsic delay of the buffer. $C_{load}$ denotes the load driven by the inverter.

- SPICE simulations refer to simulations using HSPICE unless otherwise specified.

## B. Previous Work

We summarize a few important conclusions from previous work on link insertion [8]. The basic idea behind the link based non-tree clock network construction is to obtain a non-tree by inserting cross links between nodes in an existing clock tree. A link can be modeled as a link resistor with a pair of link capacitors at the two ends. Adding only link capacitances to a clock tree may change the skew but does not change the tree topology. The original skew can be restored by tuning the tree as in conventional clock tree routing methods.

If a link resistor is inserted between a pair of nodes with equal nominal delay (or zero nominal skew), there is no change on nominal delay at any node in the clock network. If there is skew variation between the two end nodes of the link resistor, the magnitude of the variation is *always* scaled down by the link resistance. The effect of the scaling is strong when the link resistance is small or the nearest common ancestor node of the two end nodes is close to the root. If one end of the link is in subtree $T_l$ and the other end is in a disjoint subtree $T_r$, the link resistance can reduce skew variation between any pair of nodes of $T_l$ and $T_r$. However, the link resistance may worsen skew variability between nodes in some other circumstances (see [8]). The major guidelines for link insertions include:

- Links are always inserted between nodes with zero nominal skew.

- Links are preferentially inserted between node pairs which are close to each

other and their nearest common ancestor node is close to the root in the abstract topology.

- Links need to be distributed evenly in the clock network so that their skew worsening effects can cancel each other.

The main advantage of link insertion is that it provides a good trade off between skew reduction and increase in wire length. Compared to clock trees, cross link insertion can reduce the maximum skew variation by over 30% with less than 2% increase in wirelength [8]. A clock mesh can reduce the maximum skew variation by 90% but with over 60% increase in wirelength [8]. Therefore, a link based non-tree approach is an appealing choice for many ASIC designs which have relatively stringent cost/power constraints. Since such non-trees are built upon existing clock trees, this method can be easily incorporated with traditional tree based design methodology. Moreover, it can be easily extended to achieve useful non-zero clock skews. The relatively difficult non-tree delay computation is circumvented in the methods introduced in [8]. The link insertion in [25] is a special case which handles only H-trees.

Despite the advantages, previous works on link based non-tree clock network [8, 9] have a few shortcomings which hamper their applicability. The major weakness is that these works [8, 9] are limited to unbuffered clock networks. In reality, most clock networks are buffered due to the requirements on signal slew rate and maximum path delay. More importantly, buffer variations [26, 27] are usually the major contributors to clock skew variations. The effect of link insertion in buffered networks is more difficult to control than that in unbuffered cases due to the nonlinear behavior of buffer delays and the appearance of multi-driver nets. In addition to this methodological weakness, the experimental setup of [8, 9] neglected spatial correlations [28, 29] in the variation models. It has been recognized that many variations such as intra-

die process variations [29] and power supply fluctuations are spatially correlated. Link insertion for buffered clock nets was also handled in [30] (published after the preliminary version [31] of this work). We differ from [30] in the following aspects.

1. Our work addresses the issue of multi-driver nets - which is a key concern while inserting links in buffered clock nets.

2. In the experimental results section, we quantify the impact of link insertion on power dissipation.

3. We compare the results from link insertion (wire length, skew variation and power dissipation) with that of clock mesh - a popular form of non-tree based clock distribution.

C. Problem Statement

**Link Insertion for Buffered Clock Networks**

*Given a set of clock sinks $S = \{s_1, s_2, ...s_n\}$, and their load capacitances (a) construct a zero skew buffered clock tree and (b) Insert links in this clock tree such that (i) The risk of short-circuit current is avoided (ii) The tolerance of the clock net to variations in clock skew is improved and (iii) The increase in wire length/ power dissipation is minimized.*

D. Multi-driver Nets

If cross links are inserted in a buffered clock network, it is likely that a sub-net is driven by multiple buffers or drivers. This fact causes two issues which do not exist in link insertion for unbuffered clock networks. One is the risk of short circuit between the outputs of different buffers. The other is whether or not the analysis on delay

and skew in [8] is still valid in the multi-driver nets.

## 1. Short Circuit Avoidance

If the signal arrival times at the inputs of two buffers driving the same sub-net are significantly different, there is a risk of short circuit power consumption. This arrival time difference can be caused by either nominal delay difference or delay variations. Consider the example in Figure (5) where the outputs of the two buffers are initially low and then switch to high with time difference $\Delta$. There is an time interval $\Delta$ during which the output of upper buffer is high while the output of the lower buffer is low. Therefore, there could be a short circuit current flowing from the power supply to the ground through the upper buffer and then the lower buffer as indicated by the dashed line in Figure (5).
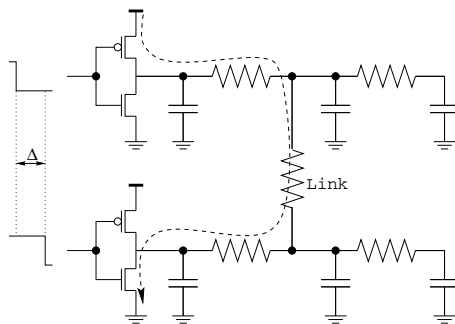


Fig. 5. If there is significant difference $\Delta$ between signal arrival time to the two drivers, there is risk of short circuit indicated by the dashed line.

However, the signal propagates with a finite time delay from one buffer to another. If this delay is greater than $\Delta$, then there is not enough time to establish the short circuit current. In other words, the output of the lower buffer may switch to high before the signal of the upper buffer propagates to it. Based on this observation, a design criterion for avoiding short circuit current between two buffers is derived as

follows.

Denote the two buffers as $B_i$ and $B_j$. Let the upper bound of the difference between signal arrival time to $B_i$ and $B_j$ be $\Delta_{ij,max}$ considering variations. The lower bound $\tau_{i \longmapsto j}$ of signal propagation delay from $B_i$ to $B_j$ can be obtained through the method detailed in [16, 32].

$$\tau_{i \longmapsto j} = \frac{\sum_{(u,v) \in path(B_i \longmapsto B_j)} R_{uv}^2 C_v}{\sum_{(u,v) \in path(B_i \longmapsto B_j)} R_{uv}} \tag{3.2}$$

where $(u, v)$ indicates two end nodes of an edge, $R_{uv}$ is the edge resistance and $C_v$ is the total capacitance downstream of node $v$. The lower bound $\tau_{j \longmapsto i}$ of signal propagation delay from $B_j$ to $B_i$ can be obtained similarly. Then, the criterion for avoiding short circuit between $B_i$ and $B_j$ is:

$$\min(\tau_{i \longmapsto j}, \tau_{j \longmapsto i}) > \alpha \Delta_{ij,max} \tag{3.3}$$

where $\alpha > 1$ is a constant used for added safety margin.

## 2.   Multi-driver Delay Analysis

In [8], it was shown that a link resistor inserted between two nodes with equal nominal delay always reduces the skew or the skew variation between them. However, this conclusion is for the single driver case. We will show that a multi-driver net can be converted to an equivalent single driver net and therefore the conclusion in [8] still holds for multi-driver nets. Consider the multi-driver net depicted in Figure (6(a)). Let $t_1(t_2)$ denote the signal arrival time at node 1(2). Without loss of generality, let $t_1 = t_2 + \Delta$, where $\Delta \geq 0$. Consider inserting a virtual resistance $R_v$ between the signal source $s_1$ and node 1 such that the delay across this virtual resistance is $\Delta$. In such a scenario, it is easy to see that the circuit can be transformed to an equivalent single driver model shown in Figure (6(b)). With the above transformation,
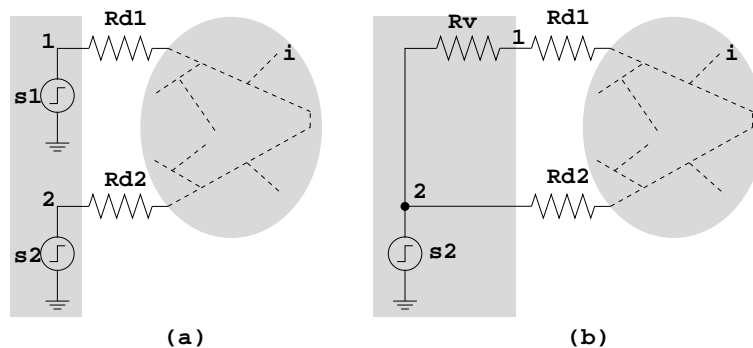
Fig. 6. The dual driver net in (a) can be converted to the single driver net in (b) when signal departure time $t_1$ at node 1 is no less than the signal departure time $t_2$ at node 2.

the analysis detailed in [8] still holds good. Since inserting a link between two equal delay nodes does not affect the delay at any node, the delay across $R_v$ can be obtained by ripping up all of the link resistance and finding the Elmore delay in the resulting tree. Therefore, the value of $R_v$ is equal to $\frac{\Delta}{C_1}$ where $C_1$ is the total downstream capacitance at node 1 for the tree.

E.  Localized Skew Tuning

For link insertion to be effective, we need to insert links between nodes with zero nominal skew [8]. However, generation of a low nominal skew tree (under a higher order delay model) is non-trivial. We will illustrate this difficulty through an example of zero skew clock tree construction in Figure (7). If zero skew has already been obtained for the buffered subtrees rooted at a1 and a2, we attempt to tune the location of the merging node m3 such that the delay from m3 to each sink (s1, s2, s3 or s4) is the same. Let *downstream delay* at a node $k$, or the delay from $k$ to sinks, be denoted as $d_k$. The location of m3 is decided based on downstream delay $d_{a1} = delay(B1) + d_{m1}$ and $d_{a2} = delay(B2) + d_{m2}$. The buffer delays $delay(B1)$ and
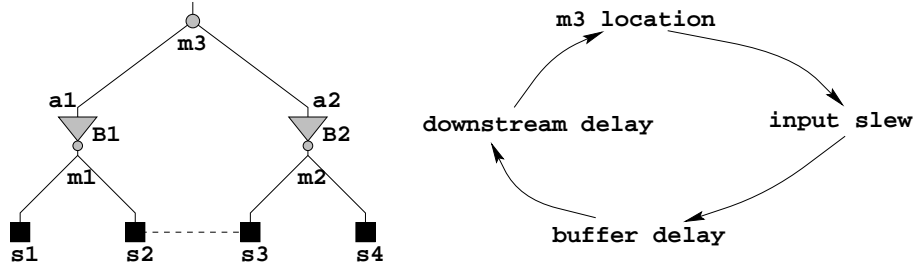
Fig. 7. Tuning the location of merging node m3 in a buffered clock tree falls into a cyclic dependency.

$delay(B2)$ depend on their input slew rates. However, the input slew rates depend on the location of merging node m3. We thus get into a *vicious cycle* that makes it very difficult to accurately find a merging node location that gives zero skew. This cycle is depicted at the right part of Figure (7).

The weakest link in this cycle is the dependence of merging node location on the downstream delay $d_{a1}$ and $d_{a2}$. Tunable delay elements were discussed in [33] as a technique used to improve the post-silicon yield. We employ this technique to break the weakest link as well as the vicious cycle. If buffer delay $delay(B1)$ and $delay(B2)$ can be tuned without affecting other delay or slew in the buffered tree, we can decide the location of m3 regardless downstream delay $d_{a1}$ and $d_{a2}$ and then obtain zero skew at sinks by tuning the buffer delays. Figure (8) shows an example of a tunable buffer containing three cascaded inverters even though different number of inverters can be employed. There is a tunable dummy capacitor $C$ between inverter $I_1$ and inverter $I_2$. For a given input slew and a given output load, the delay of the buffer can be tuned by sizing the dummy capacitor. Since the dummy capacitor is sandwiched between inverters in the buffer, changing its size does not affect any other delay or slew in the buffered tree but the buffer delay itself. In contrast to post-silicon tuning in [33], the tuning in our case is performed during the clock network layout and therefore does

not involve any testing cost.
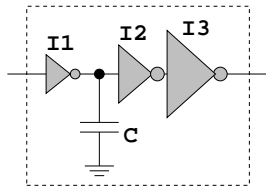


Fig. 8. Tunable clock buffer.

F.   Link Based Buffered Clock Network Construction

### 1.   Buffered Clock Tree Construction

The link based non-tree clock network construction starts with an initial buffered clock tree. There are many previous works on clock tree routing [17, 20] and buffered clock tree construction [34, 35, 36, 37] and various techniques are included in these different works. We integrate the best of them, those friendly to link insertion and the tuning technique (Section E) into a method to construct buffered clock trees. We show that the techniques are integrated in such a manner that facilitates link insertion.

Similar to previous works [34, 35, 36], we try to build a balanced tree with equal number of buffers along every source-sink path. This balanced buffered clock tree scheme is illustrated in Figure (9). Such balanced structure itself has certain tolerance to inter-die variations [34, 35]. Further, we will show later that it is friendly to link insertion.

The buffered clock tree is constructed through a bottom-up merging procedure like many traditional clock routing algorithms [17, 20, 37]. The merging order is based on the nearest neighbor method [20] which selects a pair of subtrees closest to
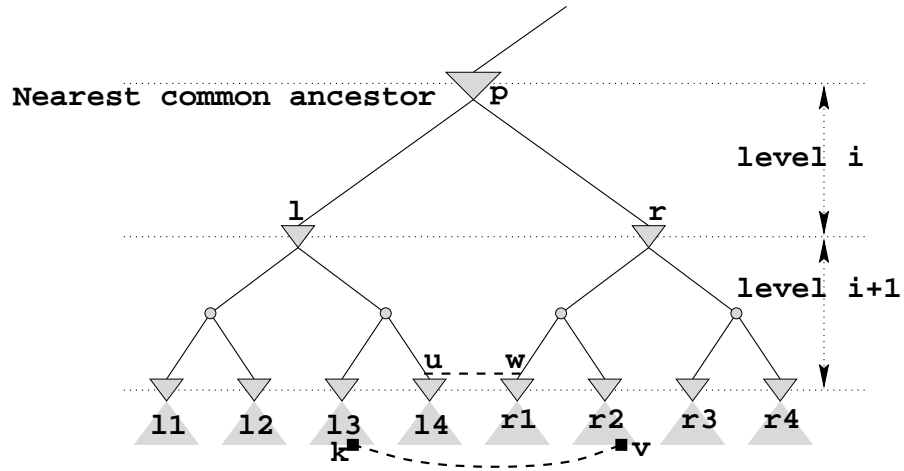
Fig. 9. Link insertion in buffered clock tree. Dashed lines indicate links.

each other for merging. In order to maintain the tree balance, we impose an extra restriction that only subtrees with fewer levels are merged first. The location of each merging node is decided by the DME (Deferred Merge Embedding) technique [17] based on the Elmore delay model. Buffers are inserted at every internal node at the same level as in Figure (9) such that the maximum load of each buffer/driver is limited. This is an indirect way to ensure proper signal slew rate [37].

In addition to the structural balance, we perform **delay balancing** [34] for subtrees at each level. After the buffer insertions, the entire tree can be partitioned into subtrees at different levels indicated by the dotted lines in Figure (9). In delay balancing, we make the delay of subtrees at the same level identical. For example, $delay(l \longmapsto u) = delay(r \longmapsto w)$ for Figure 9. The delay balancing can be achieved by using the tunable buffer detailed in Section E and sizing the dummy capacitors.

Delay balancing has several advantages. First, delay balancing results in almost equal signal arrival time at each buffer of the same level. Hence, the risk of short circuit is greatly reduced if link insertion is restricted among subtrees of the same level

according to the discussions in Section 1. The other reason is for the convenience of multilevel link insertion. Every subtree rooted at a buffer/driver becomes a zero skew subtree after delay balancing. Then, cross links can be easily inserted between subtrees at higher levels like the link between $u$ and $w$ in Figure 9. Further, as it will be explained in detail in section 2, delay balancing could lead to significant reduction in wire length.

After the buffered clock tree is constructed, a SPICE simulation is performed to obtain a precise estimation on clock skew. Usually, the skew within a subtree rooted at a buffer/driver is negligible. Since there is no buffers within such a subtree, the Elmore model provides a fairly good fidelity which is verified by SPICE simulations in [9]. However, there could be a significant delay difference between different subtrees at the same level. Thus, we perform a post-processing of delay balancing through tuning the clock buffers based on the SPICE based skew information. Compared to previous skew tuning work [38] using SPICE model, our method is much easier.

## 2.   Impact of Tunable Buffers and Delay Balancing
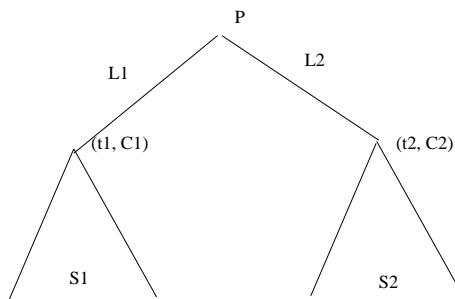


Fig. 10. Merging subtrees for zero skew tree.

In this section, we detail how delay balancing via tunable buffers helps in reducing wirelength. Consider two subtrees $S_1$ and $S_2$ that need to be merged. Let

$t_1$ ($t_2$) and $C_1$ ($C_2$) denote the downstream delay and capacitance at the root of $S_1$ ($S_2$) respectively. Let $r$ and $c$ denote the per-unit resistance and capacitance of the interconnect. The subtree characteristics are illustrated in Figure 10. Let $L_1$ and $L_2$ denote the distances between the merging point and the root of the subtrees $S_1$ and $S_2$ respectively. Let $L$ denote the distance between the root of the subtrees. In order to achieve zero skew, the lengths should satisfy [18].

$$L_1 = L\frac{(t_2 - t_1) + rL(C_2 + \frac{cL}{2})}{rL(cL + C_1 + C_2)} \tag{3.4}$$

$$L_2 = L - L_1$$

The above equations are valid when $0 \leq L_1, L_2 \leq L$. If $t_1 \gg t_2$, it is possible that $L_2 > L$. In such a case (and the converse where $L_1 > L$) we need to assign $L_1 = 0$ and $L_2 > L$. This scenario is also known as *wire snaking*. If wire snaking is required with $L_2 > L$, $L_2$ can be computed using the following formula [18]:

$$L_2 = \frac{\sqrt{(rC_1)^2 + 2rc(t_2 - t_1)} - rC_1}{rc} \tag{3.5}$$

Notice that, in case there is no snaking, the extra wirelength added as a result of merging the two subtrees equals $L$. With snaking, let $L_{snaking}$ denote the snaking length defined as $L_2 - L$. In other words:

$$L_{snaking} = (\frac{\sqrt{(rC_1)^2 + 2rc(t_2 - t_1)} - rC_1}{rc}) - L \tag{3.6}$$

In case of delay balancing, we make sure that the subtrees to be merged have equal delays (or $t_1 = t_2$. This implies that $L_1 = L_2 = \frac{L}{2}$ or there is no snaking. Delay balancing is achieved via adding an extra capacitance between inverters $I_1$ and $I_2$ in the inverter chain (Figure 8). Let the delay of inverter $I_1$ be characterized by the

following equation:

$$t_{inv} = r_b C_{load} + t_b \tag{3.7}$$

In the above equation $r_b$, $C_{load}$ and $t_b$ denote the output resistance, load capacitance and intrinsic delay of the inverter respectively. Hence, the length of the capacitance that needs to be added for delay balancing equals:

$$l_{balance} = \frac{(t_1 - t_2)}{r_b c} \tag{3.8}$$

Hence, $l_{balance}$ would be the extra wirelength spent on delay balancing. Table IV shows the comparison between delay balancing and traditional wire snaking for some typical values of subtree delay differences. The first column denotes the difference between the downstream delays of the two subtrees in psec. The second and third columns denote the values of $L_{snaking}$ and $l_{balance}$ in $\mu m$ respectively. The final column denotes the ratio of $l_{balance}$ to $L_{snaking}$. The downstream capacitances of the subtrees were set to 0.2 and 0.1 pF respectively. The distance between the subtrees ($L$) was set to 50 $\mu m$, the per unit capacitance and resistance were set to 0.39$\Omega/\mu m$ and 1.55$fF/\mu m$ respectively (parameters taken out of 65nm process [39]). The chain of inverters ($I_1, I_2, I_3$) were sized at 5x, 15x and 45x times the size of the minimum size inverters in the 65nm process. The value of $r_b$ was found to be 2224.6$\Omega$ using HSPICE simulations on a 5x size inverter using 65nm model cards from BPTM [40]. It can be seen from Table IV that delay balancing tend to consume far lesser wirelength as compared to traditional wire snaking. This is mainly due to the fact that $r_b >> r$ ($r_b$ is large since the first inverter in the chain is the smallest). Experimental results on the clock benchmarks indicate that delay balancing results in **46%** reduction in wirelength and **54%** reduction in skew on an average.

Table IV. Comparison between snaking and delay balancing.

| $(t_1 - t_2)$ | $L_{snaking}$ | $l_{balance}$ | Ratio |
|---:|---:|---:|---:|
| 5.0 | 2542.8 | 14.5 | 0.01 |
| 10.0 | 2567.8 | 29 | 0.01 |
| 20.0 | 2617.2 | 58 | 0.02 |
| 30.0 | 2665.9 | 87 | 0.03 |
| 40.0 | 2713.9 | 116 | 0.04 |

### 3.  Link Insertion

The algorithm for link insertion in buffered clock networks has some significant differences from the unbuffered case [8, 9], although they share the same top-level framework illustrated below.

1. Select the node pairs for link insertion.

2. Add link capacitance to the selected nodes and perform skew tuning to restore the original skew. The skew tuning includes two steps. First, the locations of merging nodes in each subtree rooted at a buffer/driver are tuned to restore zero skew for the subtree. Next, SPICE simulation is performed to obtain a precise inter-subtree skew estimation. And the inter-subtree skew is minimized by sizing the dummy capacitors in the tunable clock buffers. This step is the same as the post-processing in the initial buffered clock tree construction.

3. Insert link resistance into the selected node pairs. Since we always select node pairs with zero nominal skew and restore such zero skew in skew tuning of previous step, the link resistances do not affect nominal skew.

**Procedure:** $NodePairsBetweenTrees(T_l, T_r, m)$

**Input:** Two subtree $T_l$ and $T_r$,

        size indicator $m$ for each sink/buffer level

**Output:** A set $P$ of node pairs

1. $P \leftarrow \emptyset$

2. For each sink/buffer level deeper than $l$ and $r$

3.    Decompose $T_l$ to sub-subtrees $S_l = \{l_1, l_2...l_m\}$

4.    Decompose $T_r$ to sub-subtrees $S_r = \{r_1, r_2...r_m\}$

5.    Construct bipartite graph $G_{l,r}$ between $S_l$ and $S_r$

6.    $G_p \leftarrow$ MST of $G_{l,r}$

7.    For each edge $(l_i, r_j)$ in $G_p$

8.      If link between $l_i$ and $r_j$ has short circuit risk

10.        Remove $(l_i, r_j)$ from $G_p$

12.      Else if $weight(l_i, r_j) >$ threshold

13.        Remove $(l_i, r_j)$ from $G_p$

14.    $P \leftarrow P\cup$ edges in $G_p$

15. Return $P$

Fig. 11. Algorithm of selecting node pairs between two subtrees.

The most important step is node pair selection. Similar to [8, 9], the selection proceeds from the root node toward the leaf nodes recursively. In Figure (9), when an internal node $p$ is visited during this tree traversal, node pairs between its left subtree $T_l$ rooted at node $l$ and right subtree $T_r$ rooted at $r$ are selected. Every node pair between $T_l$ and $T_r$ share the same nearest common ancestor node $p$. Then, the same procedure is performed for nodes $l$, $r$ and their child nodes. The algorithm for selection of node pairs between $T_l$ and $T_r$ is shown in Figure (11). The input to this algorithm is a user-specified parameter $m$ which roughly indicates the number of pairs to be selected.

The node pair selection procedure at each sink/buffer level is derived from the MST (Minimum Spanning Tree) based algorithm in [9]. Both the left subtree $T_l$ and the right subtree $T_r$ are decomposed into $m$ sub-subtrees. In Figure (9), each subtree is decomposed into 4 sub-subtrees. Then, a bipartite graph is generated with each vertex corresponding to a sub-subtree. The weight of an edge is equal to the minimum sink/buffer distance between the two sub-subtrees it is incident on. For example, if the nearest sink pair between sub-subtree $l_3$ and sub-subtree $r_2$ is $k$ and $v$ in Figure (9), the weight of edge $(l_3, r_2)$ is equal to the distance between sink $k$ and sink $v$. Next, an MST (Minimum Spanning Tree) on this bipartite graph is obtained.

The edges in the MST correspond to candidate node pairs for the selection. These candidate edges are further pruned through a rule based iterative deletion as in line 7-13 of Figure 11. However, our algorithm differs from [9] by the fact that we employ delay balancing at levels where buffers are inserted. Such a balancing creates several pairs of zero skew nodes where a link could potentially be inserted. In addition to [9], our algorithm considers one more criteria for edge deletion. This is to ensure that there is no short circuit risk when a link is inserted for a node pair. If the inequality (3.3) is violated, the corresponding edge is removed.

Since the bipartite graph has $m$ vertices, the MST has $2m - 1$ edges. Hence, the number of node pairs selected for $T_l$ and $T_r$ at a sink/buffer level is on the order of $m$.

## G. Experiment

### 1. Experiment Setup

We use both the ISCAS89 benchmark suites as well as the well known $r1 - r5$ benchmarks [18] for our experiments. The ISCAS89 benchmark suites were synthesized using SIS [41] and placed using mPL [42]. The interconnect parameters (per-unit resistance and per-unit capacitance) were obtained from [39]. All buffers were characterized (for buffer resistance and intrinsic delays) using 65nm model cards from BPTM [40]. Our tunable buffer consists of a chain of three inverters of size 5x, 15x and 45x times that of the minimum size inverter in the 65nm process. All simulations were performed using HSPICE. The skew results presented (nominal as well as due to due to variation) refers to the maximum skew among all clock sink pairs (in other words the *global skew*) after running accurate simulation using HSPICE (since the sequential adjacency information is not available for the benchmark circuits $r1 - r5$, we used the global skew as the metric).

Our techniques were implemented in C++ and run on a Linux Work station with 2GB RAM. Clock skew variations were evaluated through Monte Carlo simulations. We consider the following sources for on-chip variations:

- Buffer channel length.

- Power supply voltage.

- Interconnect wire width variation.

- Sink load capacitance variation.

These variations are assumed to follow Gaussian distribution with standard deviations equal to 5% (for power supply, we set it to 3% of the nominal value) of their nominal values. Spatial correlations among the variations are handled by the PCA (Principle Component Analysis) method as in [29]. Power dissipation was measured by accurate HSPICE simulations. This includes all sources of power dissipation - dynamic, leakage and short-circuit.

## 2. Experiment Design

In this work, we propose three different techniques, namely:

1. Delay balancing.

2. Skew tuning via tunable buffers.

3. Link insertion for buffered clock networks.

We need to evaluate the impact of the above three methods with respect to the following design parameters:

1. Resource Consumption - consists of wire length (WL) and power dissipation.

2. Nominal Skew (NS) - the skew measured when all the parameters are set to their ideal values (no variations).

3. Skew Due to Variations - the skew measured via Monte Carlo simulations.

In all the tables presented, the following conventions will be used unless otherwise specified.

- WL denotes the wire length in $\mu m$.

- NS denotes the nominal skew. $\mu_{skew}$, $\sigma_{skew}$ and MSV denote the mean skew, standard deviation of the skew, and the maximum skew among 1000 runs of Monte Carlo. All skew results are reported in psec.

- *Pow* denotes the power dissipation in $mW$.

- BA denotes the buffer area in $\mu m^2$.

- CPU time is reported in seconds.

- Imp denotes *Improvement* in %.

## 3. Experimental Results

We first explore the impact of delay balancing and skew tuning on resource consumption and nominal skew. Table (V) gives the results for clock trees with no delay balancing and no skew tuning. In other words, this table gives the results obtained none of the techniques detailed on this work are used. The columns in Table (V) denotes the test case name, number of clock sinks, wire length, # of buffers, buffer area, power dissipation, Nominal Skew and the CPU time.

Table (VI) presents the results for clock trees with delay balancing and no tuning. For each of the parameter, we also present the improvements as compared to the ones obtained with clock trees without balancing (shown in Table V). It is evident that delay balancing alone can improve the wire length by **46%**, power by **35%** and skew by **54%**. Since we pre-characterize the buffers, the CPU time is identical to the ones when no delay balancing is done. This table gives the experimental validation for the discussions presented in Section 2.

Table (VII) presents the results for clock trees with delay balancing and tuning. For each of the parameter, we also present the improvements as compared to the ones

obtained with clock trees with balancing and without tuning. It may be noted that using skew tuning, we can reduce the nominal skew by up to **33%**. Since the wire length increase is insignificant, we use the same number of buffers. Consequently, there is no increase in area or power dissipation. The run time is determined by one run of HSPICE on the clock tree which is also very reasonable.

Table (VIII) presents the variations results obtained by running Monte Carlo simulations (1000 HSPICE runs) on clock trees obtained using delay balancing and tuning. Since such a scheme gives the best clock tree, we use this as the base case for comparison with non-trees (links and mesh). We present the mean ($\mu_{skew}$), variance ($\sigma_{skew}$) and the maximum (MSV) of the skew variations.

Table (IX) presents the variation and resource consumption results for link insertion and compares it with clock trees. With link insertion, we could reduce the maximum skew variation by over **32%** with less than **5%** increase in power dissipation. Table (X) presents similar results for clock mesh. It may be noted that clock mesh does have a better variation tolerance than links. However, the power consumption of mesh is also quite high - more than **70%** on an average.

Table V. Results for clock trees without delay balancing, without tuning.

| | No Balancing, No tuning | | | | | | |
|---|---|---|---|---|---|---|---|
| Case | #Sinks | WL | #Buffers | BA | Pow | NS | CPU |
| s9234 | 135 | 8249 | 10 | 10.99 | 1.90 | 15.31 | 0.02 |
| s5378 | 164 | 9681 | 12 | 13.18 | 2.31 | 10.97 | 0.04 |
| r1 | 267 | 11470 | 22 | 24.17 | 3.57 | 5.19 | 0.08 |
| r2 | 598 | 49607 | 114 | 125.23 | 17.25 | 57.48 | 0.94 |
| r3 | 862 | 79351 | 155 | 170.27 | 22.45 | 67.51 | 3.10 |
| r4 | 1903 | 173534 | 467 | 513.00 | 57.57 | 104.62 | 31.23 |
| r5 | 3101 | 439896 | 1544 | 1696.08 | 166.32 | 50.43 | 138.00 |
| Ave | 879 | 110255 | 332 | 364.7 | 38.77 | 44.5 | 24.77 |

Table VI. Comparison between (delay balancing, no tuning) vs (no delay balancing, no tuning).

| Case | Balancing, No tuning | | | | | | | | | | |
|------|----------|-------|---------|-------|---------|-------|--------|-------|-------|-------|--------|
| | WL | Imp | Buffers | Imp | BA | Imp | Pow | Imp | NS | Imp | CPU |
| s9234 | 5202 | 36.94 | 8 | 20.00 | 8.79 | 20 | 1.20 | 37 | 3 | 80.40 | 0.02 |
| s5378 | 6118 | 36.80 | 10 | 16.67 | 10.99 | 16.67 | 1.48 | 35.93 | 5.44 | 50.41 | 0.04 |
| r1 | 6805 | 40.67 | 16 | 27.27 | 17.58 | 27.27 | 2.44 | 31.65 | 5.22 | -0.58 | 0.08 |
| r2 | 24737 | 50.13 | 83 | 27.19 | 91.18 | 27.19 | 10.47 | 39.30 | 15.03 | 73.85 | 0.94 |
| r3 | 43178 | 45.59 | 123 | 20.65 | 135.12 | 20.65 | 16.25 | 27.62 | 34.00 | 49.64 | 3.10 |
| r4 | 92701 | 46.58 | 279 | 40.26 | 306.48 | 40.26 | 35.87 | 37.69 | 28.93 | 72.35 | 31.23 |
| r5 | 308887 | 29.78 | 949 | 38.54 | 1042.48 | 38.54 | 120.68 | 27.44 | 50.43 | 79.87 | 136.00 |
| Ave | 29687.50 | 46.33 | 86.50 | 25.34 | 95.02 | 25.34 | 11.28 | 34.87 | 15.27 | 54.35 | 5.90 |

Table VII. Comparison between (delay balancing, WITH tuning) vs (delay balancing WITHOUT tuning).

| Case | WL | Imp | Buffers | Imp | BA | Imp | NS | Imp | Pow | Imp | CPU |
|------|------|------|---------|------|---------|------|-------|-------|--------|------|--------|
| | Balancing AND tuning | | | | | | | | | | |
| s9234 | 5202 | 0.00 | 8 | 0.00 | 520 | 0.00 | 3.00 | 0.00 | 1.20 | 0.00 | 0.61 |
| s5378 | 6118 | 0.00 | 10 | 0.00 | 650 | 0.00 | 5.44 | 0.00 | 1.48 | 0.00 | 0.68 |
| r1 | 6805 | 0.00 | 16 | 0.00 | 1040 | 0.00 | 5.22 | 0.00 | 2.44 | 0.00 | 1.25 |
| r2 | 24737 | -0.48 | 83 | 0.00 | 5395 | 0.00 | 7.98 | 46.91 | 10.47 | 0.00 | 7.98 |
| r3 | 43178 | -0.51 | 123 | 0.00 | 7995 | 0.00 | 11.93 | 64.91 | 16.25 | 0.00 | 14.32 |
| r4 | 92701 | -0.30 | 279 | 0.00 | 18135 | 0.00 | 12.36 | 57.28 | 35.87 | 0.00 | 82.79 |
| r5 | 309614 | -0.24 | 949 | 0.00 | 61685 | 0.00 | 18.81 | 62.7 | 120.68 | 0.00 | 137.00 |
| Ave | 69765 | -0.22 | 209.71 | 0.00 | 13631.43 | 0.00 | 9.25 | 33.11 | 26.91 | 0.00 | 34.95 |

Table VIII. Variation results for clock trees with delay balancing and tuning.

|  | Balancing and tuning | | |
| --- | --- | --- | --- |
| Case | $\mu_{skew}$ | $\sigma_{skew}$ | MSV |
| s9234 | 31.47 | 9.41 | 61 |
| s5378 | 31.82 | 9.28 | 70 |
| r1 | 34.80 | 8.31 | 69 |
| r2 | 76.42 | 16.29 | 158 |
| r3 | 98.04 | 22.16 | 177 |
| r4 | 124.03 | 24.83 | 214 |
| r5 | 230.40 | 39.59 | 357 |
| Ave | 89.57 | 18.55 | 158 |

Table IX. Variation/resource comparison between links and clock trees.

|  | Clock trees with link insertion | | | | | | | | |
| --- | --- | --- | --- | --- | --- | --- | --- | --- | --- |
| Case | $\mu_{skew}$ | Imp | $\sigma_{skew}$ | MSV | Imp | WL | Imp | Pow | Imp |
| s9234 | 18.27 | 41.94 | 8.51 | 51 | 16.39 | 5695 | -9.48 | 1.30 | -8.85 |
| s5378 | 16.35 | 48.62 | 6.76 | 38 | 45.71 | 6712 | -9.71 | 1.60 | -8.38 |
| r1 | 9.14 | 73.74 | 4.68 | 28 | 59.42 | 7445 | -9.40 | 2.54 | -4.10 |
| r2 | 57.00 | 25.41 | 9.68 | 95 | 39.87 | 26350 | -6.52 | 10.69 | -2.10 |
| r3 | 69.07 | 29.55 | 18.41 | 142 | 19.77 | 46657 | -8.06 | 16.74 | -3.02 |
| r4 | 85.98 | 30.68 | 16.77 | 159 | 25.70 | 99731 | -7.58 | 36.96 | -3.04 |
| r5 | 171.56 | 25.54 | 35.08 | 284 | 20.45 | 35511 | -14.96 | 126.19 | -4.57 |
| Ave | 61.05 | 39.35 | 14.27 | 114 | 32.47 | 78243 | -9.39 | 28.00 | -4.86 |

Table X. Variation/resource comparison between mesh and clock trees.

| | Clock Mesh | | | | | | | | | |
|---|---|---|---|---|---|---|---|---|---|---|
| Case | Mesh Size | $\mu_{skew}$ | Imp | $\sigma_{skew}$ | MSV | Imp | WL | Imp | Pow | Imp |
| s9234 | 10x10 | 2.03 | 93.55 | 1.00 | 5.03 | 91.75 | 7836 | -50.63 | 2.46 | -105.51 |
| s5378 | 12x12 | 1.46 | 95.41 | 0.19 | 2.20 | 96.86 | 8557 | -39.87 | 2.59 | -75.00 |
| r1 | 15x15 | 3.20 | 90.80 | 1.32 | 6.99 | 89.87 | 10781 | -58.43 | 3.92 | -60.66 |
| r2 | 30x30 | 4.91 | 93.57 | 2.08 | 8.82 | 94.42 | 37146 | -50.16 | 15.72 | -50.14 |
| r3 | 35x35 | 22.62 | 76.93 | 9.92 | 45.70 | 74.18 | 81731 | -89.29 | 29.14 | -79.32 |
| r4 | 45x45 | 37.22 | 69.99 | 12.41 | 78.50 | 63.32 | 123022 | -32.71 | 56.23 | -56.76 |
| r5 | 80x80 | 116.40 | 49.48 | 38.67 | 225.96 | 36.71 | 561616 | -81.82 | 199.25 | -65.11 |
| Ave | 32.5x32.5 | 26.83 | 81.39 | 9.37 | 53.31 | 78.16 | 118706 | -57.56 | 18.34 | -70.36 |

CHAPTER IV

METHODOLOGY AND ALGORITHMS FOR ROTARY CLOCKING

Rotary clocking has been shown to be a promising new clocking scheme that handles both power and variation issues [10]. In this chapter, we discuss the issues involved in using the current CAD flows for rotary clocks. We detail alternative flow and algorithms.

A.   Previous Work
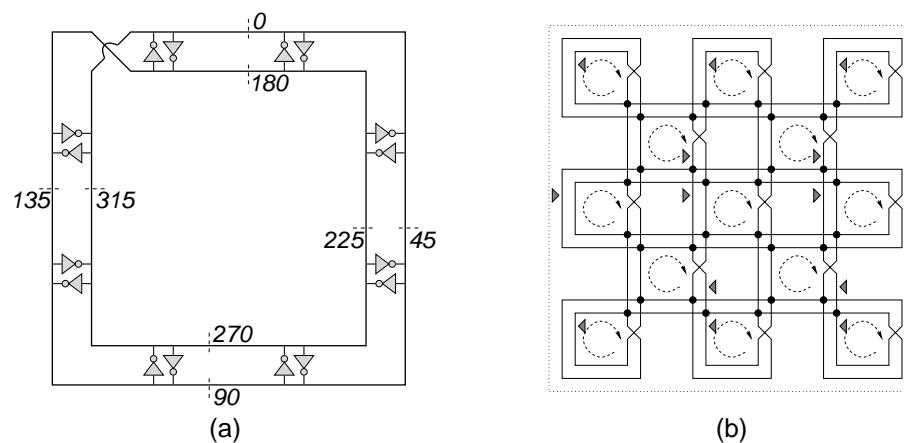


Fig. 12. (a) A rotary clock ring. The numbers indicate relative clock signal phase. (b) An array of 13 rotary clock rings. The small triangles points to the equal-phase points for the 13 rings.

In order to solve the power and the variation problem more effectively, several novel clocking technologies have been developed [10, 43, 44]. Among them, rotary traveling wave clock [10] is a promising approach. The basic component of a rotary clock is a pair of cross-connected differential transmission line circles, namely a rotary clock ring (as shown in Figure 12(a)). A clock signal propagates along the ring without

termination so that the energy can be recirculated and the charging/discharging power dissipation is greatly reduced. A recent study [45] shows that rotary clocks can reduce power dissipation by 70% compared to conventional clock networks. The measurement results from a test chip also showed that a low skew variation of $5.5ps$ at $950MHz$ can be achieved [10]. Rotary clock can provide uniform clock signal amplitude in contrast to the non-uniform amplitude in standing wave clock [43].

There is one technical hurdle that prevents wide applications of the rotary clock: the clock signal has different phases at different locations on the rotary clock ring. If zero skew design is insisted, the usage of rotary clocks would be very restrictive. Hence, non-zero intentional skew design is a better approach to fully utilize the rotary clock. Unlike the intentional skew design in the conventional clocking technology where no restrictions are imposed on the flip-flop locations, the skew at each flip-flop has to be matched with a specific location at the rotary clock ring. This requirement forms a difficult chicken-and-egg problem: the flip-flop placement depends on skew optimization while it is well known that skew optimization depends on flip-flop locations. This is quite different from traditional intentional skew designs [46] where the placement does not depend on skew optimization.

The goal of this work is to break this technical hurdle so that rotary clocks can be easily deployed in practice to alleviate the power and variation issues. We make the following contributions in this work.

- A relaxation technique based on flexible tapping is suggested to break the loop in the chicken-and-egg problem.

- An integrated placement and skew optimization methodology is proposed. This methodology has the advantage that it fits well with the current CAD flow and the placers can be used without any change.

- A min-cost network flow algorithm is found to assign flip-flops to the rotary clock

rings so that the movement of flip-flops has the least disturbance to traditional placement.

- A pseudo net technique is introduced to guide flip-flops toward their preferred locations without intrusive disturbance to traditional placement.

- A cost driven skew optimization formulation is developed to reduce the connection cost between flip-flops and their corresponding rotary clock rings.

- We develop an Integer Linear Programming (ILP) formulation to minimize the maximum capacitance loaded at any rotary ring. Since the operating frequency is inversely proportional to the load capacitance, this formulation could be used in delay critical designs. We also detail a fast and effective heuristic used to solve the formulation.

B.   Rotary Traveling Wave Clock and Traditional Design Flow

In this section, we discuss the basics of rotary clocking, its advantages, whether a rotary clock can fit into a traditional design flow and if not, what are the difficulties. The basic component of a rotary clock is a pair of cross-connected transmission line circles as shown in Figure 12(a). In the rotary clock ring, an oscillation can start spontaneously upon any noise event [10]. When the oscillation is established, the square wave signal can travel along the ring without termination. An arbitrary point on the ring can be designated as the reference point with clock signal delay $t = 0$ and clock phase $\phi = 0$. Starting from this reference point, the clock signal travels along the ring and reaches back to the reference point with delay equal to clock period $T$ and phase $\phi = 360$. The numbers in Figure 12(a) indicate clock signal phases. Clock signal delay $t$ and clock signal phase $\phi$ can be converted to each other by $\frac{\phi}{360} = \frac{t}{T} - \lfloor \frac{t}{T} \rfloor$.

The energy loss due to the wire resistance is compensated by the anti-parallel inverters as shown in Figure 12(a). In addition, these inverter pairs help to achieve phase locking as the phases of the two circles at the same location are always opposite. In order to maintain uniform capacitance distribution along the ring, dummy capacitive load needs to be inserted at places where no flip-flops exist. In chip level designs, multiple rotary clock rings can be connected together to form an array as shown in Figure 12(b), where the dashed arrows indicate the signal propagation directions and the small triangles indicate equal phase locations for all rings.

A rotary clock has the advantage of both low power dissipation and low skew variation. It consumes less power as the energy is recirculated along the ring as opposed to energy loss during the charging/discharging through transistors in conventional clocking. In the rotary clock ring array (Figure 12(b)), the phase averaging at the junction points can reduce skew variation remarkably.

In spite of the appealing advantages, the rotary clocking scheme is not compatible with existing design flows. Consider the cross-coupled rings shown in Figure 12(b). Since at each spot on a rotary clock ring, the clock signal has a distinct phase, a zero clock skew design implies that only one spot on each ring can be utilized. In Figure 12(b), there are 13 rings and there are only 13 useful spots for a zero clock skew design. Obviously, such usage of rotary clock is very inefficient. In order to fully utilize rotary clock, intentional skew design is a much better choice. Even with intentional clock skews, rotary clocking poses an important problem. A typical intentional skew design flow, which is employed in IBM high performance ASIC designs [46] proceeds in the order of the following stages.

1. Placement. In placement [47, 48], cells are placed in a non-overlapping manner so that an objective function, such as the total signal net wirelength, congestion, critical path timing or a combination of them, is minimized.

2. Clock skew optimization. For intentional skew designs, clock signal delay target to each flip-flop is found so as to minimize clock period or maximize timing slack, subject to long path and short path constraints. Since the long path and short path constraints depend heavily on cell and flip-flop locations, placement information is essential in order to perform skew optimization. We will discuss skew optimization in Section G.

3. Clock distribution network synthesis. In this stage, a clock distribution network layout is generated to approximately deliver intentional skews [46], which correspond to the clock delay targets obtained in skew optimization. Of course, the clock distribution network layout depends on flip-flop locations.

The feasibility of this flow is based on its one-way dependency that each stage relies on the result of the previous stages, but not vice versa. More specifically, the placement (with the inclusion of flip-flops), does not depend on skew optimization or clock distribution network synthesis. Likewise, skew optimization does not depend on clock distribution network synthesis.

Rotary clock is usually designed independently. In placement, each flip-flop needs to be placed at a rotary clock ring and the clock phase at its location has to match the clock signal delay target for the flip-flop. This requirement causes a cyclic dependency. The flip-flop placement depends on its clock signal delay target, which is generated by skew optimization. But skew optimization is always dependent on placement. This chicken-and-egg problem has to be solved to enable the application of rotary clocking technique.

## C.  Relaxation via Flexible Tapping

For a complex constrained optimization problem, relaxation is an effective technique to handle troublesome constraints. The difficulty of applying rotary clock can be alleviated if we relax the constraint which requires each flip-flop to be attached exactly on a rotary clock ring. For a flip-flop at an arbitrary location $(x_f, y_f)$, we can always find a tapping point $p$ on a rotary clock ring and deploy a buffer at $p$ to drive the flip-flop through a wire such that clock signal delay $t_f$ at $(x_f, y_f)$ satisfies a pre-specified clock delay target $\hat{t}_f$ for the flip-flop. Of course, we do not want the flip-flop to be too far away from the ring. Otherwise, the long wire between the tapping point and the flip-flop may cause significant power and variability degradation that it becomes meaningless to use rotary clock. On the other hand, if a flip-flop is very close to its tapping point on the ring, the buffer can be omitted. The wirelength between the tapping point $p$ and the flip-flop can be counted as a cost to be minimized in placement and skew optimization. The approach of transforming troublesome constraints to cost is very similar to Lagrangian relaxation.
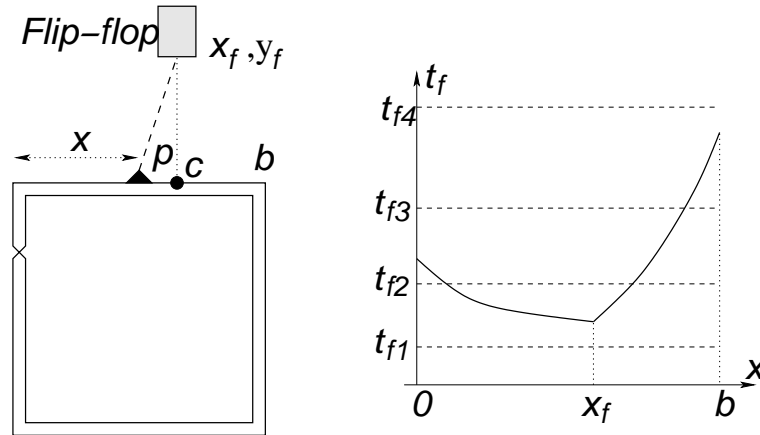


Fig. 13.  The tapping point $p$ for a flip-flop can be found by solving the delay satisfying clock signal delay target.

Now we will show how to find the location of the tapping point so that the delay target $\hat{t}_f$ for the flip-flop at $(x_f, y_f)$ can be satisfied. We illustrate this procedure through an example in Figure 13. A rotary clock ring is implemented in square shape in layout and is composed by four inside segments and four outside segments, as shown in Figure 13. Without loss of generality, we only consider the case when the tapping point is on the top segment. Other cases can be derived in an almost identical manner. We assume that the left end of the segment is set at coordinate $(0, 0)$, the location for the right end, the flip-flop and the tapping point are represented as $(b, 0)$, $(x_f, y_f)$ and $(x, 0)$, respectively. If the delay of the clock signal at $(0, 0)$ is $t_0$, then the delay at $p$ can be expressed as $t_0 + \rho x$ [10] with $\rho$ being a positive constant. We denote the distance between the tapping point and the flip-flop as $l$, assuming wire resistance and capacitance per unit length are $r$ and $c$, respectively. Let $C_{flip-flop}$ denote the input capacitance of the flip-flop. In order to satisfy the clock signal delay target at the flip-flop, the clock signal delay $t_f$ has to satisfy:

$$t_f(x) = t_0 + \rho x + \frac{1}{2}rcl^2 + rlC_{flip-flop} = \hat{t}_f \qquad (4.1)$$

Since $l = |x - x_f| + y_f$, $l$ is a function of $x$. The location of the tapping point can be obtained by solving the above equation.

Figure 13 shows an example of curve $t_f(x)$ which is composed by two parabolas joining at $x = x_f$. The function $t_f(x)$ can be decomposed into a quadratic function plus the term of $|x - x_f|$. The quadratic function leads to a single parabola. However, the term of $|x - x_f|$ consists of two pieces of linear parts with a non-differentiable joint point at $x = x_f$. Therefore, the overall shape of the $t_f(x)$ curve becomes two pieces of parabolas joining at $x = x_f$. Depending on the value of $\hat{t}_f$, there are four cases for solving Equation (4.1).

- Case 1: $\hat{t}_f$ is very small like $t_{f1}$ in Figure 13. There is no direct solution for this

case. This case can be circumvented by reducing $t_0$ by integer number of clock period time $T$. Note that such reduction does not affect clock phase. This is equivalent to lowering the curve $t_f(x)$ by multiple $T$ and eventually results in one of the following three cases. Obviously, the number of $T$ for the reduction needs to be minimized.

- Case 2: $\hat{t}_f$ is moderately small like $t_{f2}$ in Figure 13. There are two solutions in the case and the solution with smaller wirelength is selected.

- Case 3: $\hat{t}_f$ is at middle level like $t_{f3}$ in Figure 13. There is a unique solution.

- Case 4: $\hat{t}_f$ is large like $t_{f4}$ in Figure 13. There is no direct solution for this case. However, we can choose $(b, 0)$ as the tapping point and intentionally introduce wire detour between $p$ and the flip-flop so that delay target $\hat{t}_f$ is satisfied. This is almost the same as the wire snaking in clock tree routing [18].

After the tapping points on each of the eight segments are calculated, the one leading to the minimum wirelength is selected as the tapping point for the ring. The actual wirelength for achieving the clock signal delay target is defined as the tapping cost. Note that we could also use a buffer to drive the signal from point $p$. If needed, equation (4.1) can be easily modified to take care of the buffer delay.

It may be noted that in a rotary ring, a phase and its complementary phase (two phases are complementary to each other if they are 180 degrees apart, for example 90 and 270 are complementary phases) are available at points that are physically close to each other. Let $\phi_1$ and $\phi_2$ denote the two complementary phases available at a points $p_1$ and $p_2$ in the rotary ring. If two flip-flops $F_1$ and $F_2$ are both assigned to $p_1$, then one can connect $F_1$ to point $p_1$ (with phase $\phi_1$), $F_2$ to point $p_2$ (with phase $\phi_2$) and assign opposite polarities to $F_1$ and $F_2$ (that is we can make one positive-edge triggered and another one as negative edge triggered).

D.   Proposed Methodology

The flexible tapping technique breaks the cyclic dependency between the placement and skew optimization. It also facilitates a new methodology flow as shown in Figure 14, in which skew awareness for the placement is achieved indirectly through a pseudo net technique. By doing so, the traditional placement methods can be used without any change. This is an appealing feature because placement is a much more complicated problem than skew optimization.
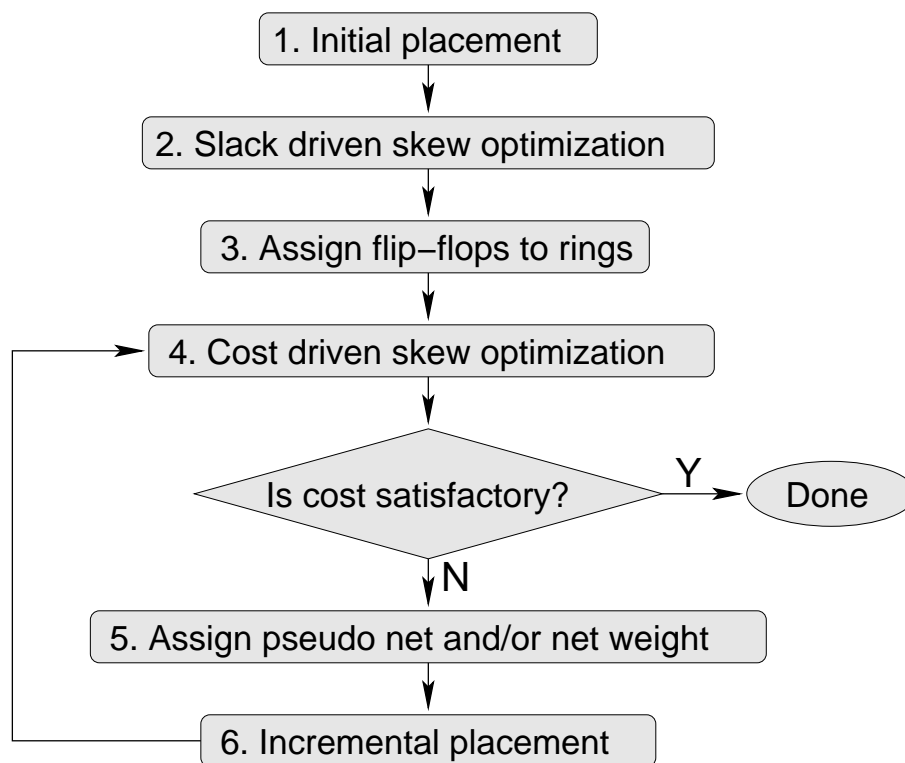


Fig. 14. Proposed methodology flow.

The first two stages are almost the same as the traditional flow. The initial placement can be implemented with any existing placement method [47, 48] without special considerations of flip-flop locations or their skews. In stage 2, skew optimiza-

tion [1] is performed based on the placement of stage 1 to maximize the timing slack. The details of this part will be described in Section G.

In stage 3, each flip-flop is assigned to a ring of the rotary clock ring array. This assignment only establishes an association between a particular flip-flop to a ring and does not change the flip-flop location. When a flip-flop is assigned to a specific ring, the corresponding tapping cost can be computed according to Section C. Depending upon the design objective, we propose two different techniques for flip-flop assignment:

1. A network flow based assignment algorithm which aims at minimizing the total tapping length subject to capacity constraints. This technique is detailed in section E.

2. An Integer Linear Programming (ILP) based approach that aims at minimizing the maximum capacitance loaded at any of the rotary rings. This technique (detailed in section F) can be used in high speed designs.

After each flip-flop is assigned to a ring, another skew optimization can be performed to reduce the tapping cost. This is somewhat different from traditional skew optimization and will be discussed in details in Section G. After stage 4, the overall cost is evaluated as a weighted sum of total tapping cost and traditional placement cost, which is usually total signal wirelength. If the overall cost is sufficiently small, this flow is completed. Otherwise, the flow proceeds to stage 5.

Since the initial placement is based on the traditional objectives such as signal wirelength and ignores tapping cost, it is quite likely that the tapping cost is very high when we enter stage 5 for the first time. In order to reduce tapping cost, we insert a pseudo net between each flip-flop and its ring. The flip-flops can be pulled toward their associated rings in the placement stage 6. Since stage 6 is an incremental placement, it normally runs considerably faster than the initial placement. Of course,

the incremental placement is preferred to be a stable one [47], i.e., small changes on the netlist should not cause dramatic change on the placement result.

E.   Flip-flop Assignment to Minimize Tapping Cost

In stage 3 of the above flow, each flip-flop needs to be assigned to a ring in the rotary clock ring array. It is required that the assignment minimizes the tapping cost defined in Section C. We denote the tapping cost as $c_{i,j}$, when a flip-flop $i$ is assigned to ring $j$. Each ring $j$ has limited space and can accommodate no more than $U_j$ flip-flops. We introduce a decision variable $x_{i,j}$: if flip-flop $i$ is assigned to ring $j$, $x_{i,j} = 1$, otherwise $x_{i,j} = 0$. The flip-flop assignment problem can then be formulated as the following 0-1 programming problem.

$$\text{Minimize} \quad \sum_{i,j} c_{i,j} x_{i,j}$$

$$\text{Subject to} \quad \sum_j x_{i,j} = 1 \quad \forall i$$

$$\sum_i x_{i,j} \leq U_j \quad \forall j$$

$$x_{i,j} \in \{0,1\} \quad \forall i,j$$
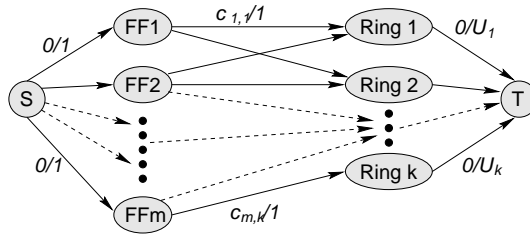


Fig. 15. Min-cost network flow model for flip-flop assignment. Each arc is associated with cost/capacity.

This assignment problem can be solved using min-cost network flow model [49]

as shown in Figure 15. The vertices in the network include a column of flip-flop vertices, a column of ring vertices, a source vertex and a target vertex. There is an arc from a flip-flop vertex to a particular ring vertex only if the corresponding flip-flop is considered to be a potential candidate of the ring. If a flip-flop and a ring are too far away from each other, it is not necessary to insert an arc between them. Each arc between a flip-flop vertex $i$ and a ring vertex $j$ has a cost of $c_{i,j}$. The rest arcs have zero cost. Each arc from a ring vertex $j$ to the target vertex has a capacity of $U_j$. The other arcs have a capacity of 1. It is well known that this min-cost network flow problem can be solved optimally in polynomial time [49].

## F. Flip-flop Assignment to Minimize Load Capacitance

In this section, we present an alternative formulation that can be used in place of the one discussed in section (E). The frequency of operation of the rotary clock is given by [50]:

$$f_{osc} = \frac{1}{2\sqrt{L_{total}C_{total}}} \tag{4.2}$$

$C_{total}$ consists of two components - the ring capacitance and the capacitance of the load that the ring drives. The latter shall hence forth be referred to as load capacitance. Since the ring capacitance for a given ring dimension is a constant, we can minimize $C_{total}$ by minimizing the load capacitance. If the design objective is to run the maximum possible frequency, then the load capacitance at the rings is a more relevant optimization objective. The network flow formulation discussed in section (E) attempts to distribute the flip-flops uniformly across the rotary rings while optimizing the tapping length. While this is ideal if the design objective is to minimize the tapping length, it is not a direct measure of the load capacitance.

We present an alternative formulation which takes into account the load capaci-

tance at the rotary rings. Let $C_p^{ij}$ denote the load capacitance of a flip-flop $i$ when it is assigned to a ring $j$. This capacitance includes both the interconnect capacitance as well as the flip-flop input capacitance (or buffer capacitance). Let $x_{ij}$ denote the indicator variable that is set to one if flip-flop $i$ is assigned to ring $j$ and zero otherwise. Then the formulation to minimize the maximum load capacitance can be stated as follows:

$$\text{min max} \quad \sum C_p^{ij} x_{ij} \tag{4.3}$$
$$\sum_{\forall j} x_{ij} = 1 \forall i$$
$$x_{ij} \in \{0, 1\}$$

The following key observations can be made about formulation (4.3):

- The cost $(C_p^{ij})$ is a direct measure of the load capacitance in contrast to the cost used in formulation (4.2)

- The formulation is an integer programming (ILP) problem. ILP in general is NP-hard and hence there is a need to employ fast and effective heuristics.

### 1.  Solution by LP-relaxation

LP-relaxation has been used to solve a certain class of combinatorial optimization problems like the set cover [51]. The basic steps involved in LP-relaxation are as follows:

1. Relax the integer constraints (usually 0-1 constraints on decision variables) to continuous constraints. For example an integer constraint $x_{ij} \in \{0, 1\}$ would be replaced by $0 \leq x_{ij} \leq 1$.

2. Solve the resulting LP. For a minimization problem, the optimal solution to the

LP gives a lower bound on the optimal solution to the ILP. This is due to the fact that any feasible solution to the ILP is also a feasible solution to the LP.

3. Now round the LP solution to the get an integer solution.

The key to any LP-relaxation procedure is the rounding process. The rounding process should be such that (a) Feasibility of the ILP is maintained and (b) The deviation of the objective function is minimized. With the above two restrictions in mind, we employ a rounding procedure which shall henceforth be referred to as **greedy rounding**.

Let $I$ denote the set of flip-flops, $J$ the set of rotary rings, $X^{lp} = \{x_{ij}^{lp}\}$ the solution obtained from the LP-relaxation and $X^{ilp} = \{x_{ij}^{ilp}\}$ the ILP solution obtained on LP-rounding. For feasibility, we need to make sure that each flip-flop is assigned to exactly one ring. This is done by ensuring upon rounding $x_{ij}^{ilp}$ is set to exactly one $j \in J$.

The greedy rounding procedure is described in Figure (16). If the LP solution also happens to be integral, we retain it. If not each flip-flop $i$ is assigned to the ring $j$ whose corresponding assignment variable $x_{ij}^{lp}$ is maximum. Hence our procedure is referred to as greedy rounding. The complexity of the rounding procedure is linear in the number of flip-flops and the number of rings. Since the number of rings is much smaller than the number of flip-flops and the solution to LP generally runs in linear time (in practice), the overall procedure of greedy rounding is linear in the problem size.

Let $OPT(LP)$ denote the optimum solution of the LP-relaxation and $SOLN(ILP)$ denote the solution of obtained after solving the ILP (by any procedure). Then we

define *integrality gap IG* as:

$$IG = \frac{SOLN(ILP)}{OPT(LP)} \tag{4.4}$$

The following observations can be made about $IG$:

1. $IG \geq 1$, since the LP solution is always lower than the ILP solution.

2. ILP in general is NP-complete. But, whether the ILP described in Equation (4.3) can be solved optimally in polynomial time remains open. Since we currently do not know the optimal solution, $IG$ acts as a good base case for comparison.

3. The value of $IG$ should not be interpreted in an absolute sense. For example, $IG = 1.40$ does NOT mean that the solution of the heuristic is 40% away from optimal value.

In order to compare the efficacy of the proposed heuristic, we ran the same formulation using a public domain ILP-solver [52]. Table (XI) presents the comparison between greedy rounding and ILP-solver. The comparisons are made in terms of both run-time and quality of solution (measured by the Integrality Gap). While greedy rounding produced a solution within few seconds, the ILP-solver took several hours. We bounded the simulation time for the ILP-solver to 10 hours and report the best solution that it produced within this time. For 3 of the test cases, the ILP-solver did not produce a feasible solution. For the remaining 2 the greedy rounding outperformed ILP-solver by a significant margin. This is not unexpected since the ILP solver is generic in nature whereas our rounding procedure exploits the problem structure.

It was observed that the ILP formulation reduces the maximum capacitance significantly. But this reduction comes at the expense of increased signal and clock

Table XI. Integrality gap of greedy rounding and ILP-solver.

| Circuit | Greedy Rounding | | ILP-Solver | |
|---|---|---|---|---|
| | IG | CPU(s) | IG | CPU |
| s9234 | 1.32 | 0.25 | 1.83 | > 10hrs |
| s5378 | 1.57 | 0.31 | 22.05 | > 10hrs |
| s15850 | 1.32 | 2.0 | – | > 10hrs |
| s38417 | 1.23 | 6.10 | – | > 10hrs |
| s35932 | 1.63 | 13.10 | – | > 10hrs |

wire length. The details are discussed in section (H).

---

**Procedure: Greedy Rounding**

---

**Input:** $X^{lp} = \{x_{ij}^{lp}\}$:    Solution for the relaxed LP

I - set of flip-flops, J - set of rings

**Output:** $x_{ij}^{ilp}$:    Solution to the ILP

---

1. For each $i \in I$ do

1.1 If $x_{ij_1}^{lp} = 1$ for some $j_1 \in J$,

$$x_{ij_1}^{ilp} = 1 \text{ and } x_{ij}^{ilp} = 0 \ \forall j \neq j_1$$

1.2 Else

Find $j_{max} \in J$ such that

$$x_{ij_{max}}^{lp} \geq x_{ij}^{lp} \forall j \in J$$

$$x_{ij_{max}}^{ilp} = 1 \text{ and } x_{ij}^{ilp} = 0 \ \forall j \neq j_1$$

2.  Return $X^{ilp} = \{x_{ij}^{ilp}\}$

---

Fig. 16. Greedy rounding algorithm.

G.   Skew Optimization

Skew optimization is an important part of the proposed flow. The skew optimization in stage 2 is the same as the max-slack version of the traditional method [1] and we summarize it here for completeness. If two flip-flops $i$ and $j$ are said to be *sequentially*

*adjacent* if they have only combinational logic between them. Sequential adjacency is denoted by $i \longmapsto j$. Let $D^{ij}_{max}$ ($D^{ij}_{min}$) denote the maximum (minimum) combinational logic delay between $i$ and $j$. Let $\hat{t}_i$ denote the clock signal arrival time at $i$, $t_{setup}$ ($t_{hold}$) the setup (hold) time and $T$ the clock period. Then the max-slack version of skew optimization can be formulated as [1]:

$$\text{Maximize} \qquad\qquad M \qquad\qquad\qquad\qquad (4.5)$$

$$\text{Subject to}\ \ \hat{t}_i - \hat{t}_j + M \leq T - D^{ij}_{max} - t_{setup}\ \ i \longmapsto j \qquad\qquad (4.6)$$

$$\hat{t}_i - \hat{t}_j \geq M + t_{hold} - D^{ij}_{min} \qquad i \longmapsto j \qquad\qquad (4.7)$$

where $M$ is the slack. Inequalities (4.6) and (4.7) are referred to as the long path constraint and short path constraints, respectively. It has been shown that this problem can be solved using linear programming [1] or graph based algorithms [19, 23].

We propose a cost driven method so that skew optimization can be leveraged to assist placement on reducing the total tapping cost. The computation of the tapping cost (Section C) is based on a known clock signal delay target while the delay target is a decision variable in skew optimization. Therefore, we try to minimize the tapping cost indirectly by finding clock signal delay targets such that the tapping point can be moved to the flip-flop as close as possible. For example, in Figure 13, if the delay target of the flip-flop can result in tapping point at $c$, then the tapping cost is minimized. In other words, if the actual delay to a flip-flop $i$ is $t_i$ through tapping point at $c$, we try to make the delay target $\hat{t}_i$ to be as close to $t_i$ as possible.

For flip-flop $i$, we first find the closest point $c$ on its ring and the distance between $i$ and $c$, which is the shortest distance between $i$ and the ring, is denoted as $l_i$. The delay $t_i$ at $i$ through tapping point at $c$ depends on the reference clock signal delay on the rotary clock rings. We can arbitrarily choose a set of equal phase points for all the

rotary clock rings as reference points like the small triangular spots in Figure 12(b). Let the clock signal delay at the reference points be $t_{ref}$. If the delay from the reference point to $c$ is $t_{ref,c}$, then the clock signal delay at $c$ is $t_c = t_{ref} + t_{ref,c}$. The delay from $c$ to $i$ is $t_{c,i} = \frac{1}{2}rcl_i^2 + rl_iC_{flip-flop}$ which is very similar to Equation (4.1). Hence, the clock signal delay at $i$ is $t_i = t_c + t_{c,i}$, If the difference $|t_i - \hat{t}_i|$ is minimized, there is a good chance that the tapping point is the closest to $c$ and the flip-flop. When a flip-flop $i$ is far from its ring, i.e., $t_{c,i}$ is large, it is especially desired that the tapping point is closest to $c$. Therefore, $|t_i - \hat{t}_i| + t_{c,i}$ is minimized in the cost driven skew optimization.

$$
\begin{aligned}
&\text{Minimize} && \Delta \\
&\text{Subject to} && \hat{t}_i - \hat{t}_j + M \leq T - D_{max}^{ij} - t_{setup} \quad i \longmapsto j \\
& && \hat{t}_i - \hat{t}_j \geq M + t_{hold} - D_{min}^{ij} \quad\quad i \longmapsto j \\
& && t_{ref} + t_{ref,c} + 2t_{c,i} - \hat{t}_i \leq \Delta \quad\quad \forall i \\
& && \hat{t}_i - t_{ref} - t_{ref,c} \leq \Delta \quad\quad\quad \forall i
\end{aligned}
$$

where $\Delta$ is the maximum difference and $M$ is a pre-specified slack. The constraint from the two inequalities in this formulation is equivalent to $|t_i - \hat{t}_i| + t_{c,i} \leq \Delta$. Obviously, this problem can be solved through linear programming [1].

Alternatively, the skew optimization problem can be formulated to minimize a weighted sum of the differences as follows.

$$
\begin{aligned}
&\text{Minimize} && \sum_{\forall i} w_i \delta_i \\
&\text{Subject to} && \hat{t}_i - \hat{t}_j + M \leq T - D_{max}^{ij} - t_{setup} \quad i \longmapsto j \\
& && \hat{t}_i - \hat{t}_j \geq M + t_{hold} - D_{min}^{ij} \quad\quad i \longmapsto j \\
& && t_i - \hat{t}_i \leq \delta_i \quad\quad\quad\quad \forall i
\end{aligned}
$$

$$\hat{t}_i - t_i \leq \delta_i \qquad\qquad \forall i$$

where $\delta_i$ is the difference for flip-flop $i$ and $w_i$ is its weighting factor. A natural choice of the weighting factors is to let $w_i = l_i$, as we wish to focus our effort on those flip-flops far away from their rings. Again, this problem can be solved directly through linear programming [1].

## H.   Experimental Results

The proposed methodology and algorithms are tested on the ISCAS89 benchmark suite. The benchmark characteristics are summarized in Table (XII). The first four columns indicate the circuit name, number of standard cells, number of flip-flops and the number of nets respectively. In the fifth column of Table (XII), we report average source-sink path length in conventional clock trees [17, 20] for reference. The number of rotary rings for each test case is indicated in the final column. The rotary clock ring arrays are generated as in [10]. The operating frequency was set at 1GHz. The circuits are synthesized using SIS [41]. The main algorithms are implemented in C++. The initial placement as well as the incremental placement are obtained from an academic placement tool mPL [48, 42]. Soplex was used to solve the LP-relaxation problem [53]. All experiments are performed on a Pentium 4 workstation running Linux operating system with 1 GB RAM. The interconnect parameters are obtained from *bptm* [40]. The skew permissible ranges can be computed using any static timing analysis tool as detailed in  [1]. We used the Elmore delay model [16] in our static timing analyzer. However, our techniques are generic and can be extended to more accurate timing analysis tool without any changes in the underlying skew optimization algorithms or the overall flow.

To the best of our knowledge, there is no published work on placement and skew

Table XII. Testcases. PL is the average source-sink path length in conventional clock trees [17, 20].

| Circuit | #Cells | #Flip-flops | #Nets | PL($\mu m$) | # Rings |
|---------|--------|-------------|-------|-------------|---------|
| s9234   | 1510   | 135         | 1471  | 2471        | 16      |
| s5378   | 1112   | 164         | 1063  | 2718        | 25      |
| s15850  | 3549   | 566         | 3462  | 5175        | 36      |
| s38417  | 11651  | 1463        | 11545 | 8261        | 49      |
| s35932  | 17005  | 1728        | 16685 | 8290        | 49      |

optimization for rotary clocking. There are three issues which we care about:

1. Each flip-flop needs to be close to the ring it associated with so that the off-ring variation effect is negligible

2. Moving flip-flops toward their associated rings should not degrade signal wirelength significantly and the total wirelength including tapping wirelength needs to be minimized.

3. If the design objective is speed, then the maximum load capacitance at any of the rotary ring should be minimized.

Table (XIII) gives the results for the base case. These results (base case) are obtained by running the flip-flop assignment algorithm using network flow at stage 3 of our overall flow (indicated in Figure (14)). In all the tables shown, AFD denotes the Average Flip-flop Distance and WL the wire length. All wire lengths are reported in $\mu m$, capacitances are reported in $pF$ and power in $mW$. Table (XIII) presents the AFD, tapping wirelength, signal wirelength, total wirelength, power dissipation in the clock net, power dissipation in the signal net and total power dissipation for the

base case. It can be seen that the average flip-flop distance is significantly smaller than the average source-sink path length in conventional clock trees [17, 20] (as shown in the rightmost column of Table (XII)). The power dissipation is obtained by the technique(s) detailed below. The power dissipation in the clock net includes the dynamic power dissipated in the tapping wires from the rotary ring as well as the power dissipated in the flip-flops. The power dissipated in the signal length includes the power dissipated in the interconnect, logic gates as well the the buffers. The power dissipation is measured using the following formula.

$$P_{dynamic} = \frac{1}{2}\alpha V_{dd}^2 f_{clk} C_{load} \qquad (4.8)$$

In the above equation, $\alpha$ denotes the switching activity, $f_{clk}$ the clock frequency, and $C_{load}$ the total capacitive load and $V_{dd}$ the supply voltage. For the clock net, $\alpha$ is set to 1. Estimating $\alpha$ for signal net is a hard problem and setting it to 0.15 usually gives a reasonable approximation [5]. For clock nets, we know the actual interconnect capacitance and the flip-flop capacitance accurately and hence estimating the power is straightforward. The capacitance in the signal net consists of three components: (a) the interconnect capacitance (b) the input capacitance of logic gates and (c) the input capacitance of the buffers used in the signal net. The first two capacitances are easy to estimate since we have a placed/mapped design. To estimate the number of buffers in the signal net, we use the technique detailed in [54]. The above technique estimates the buffer delay (while estimating the number of buffers inserted) at an early stage (floorplan) with a reasonable accuracy. Thus we estimate the dynamic power dissipated at the clock and signal net and sum them up to get the total power. The total leakage power in a circuit can be approximated to [5]:

$$P_{leakage} = V_{dd}I_{off}(S + N_F S_F) \qquad (4.9)$$

In the above equation $I_{off}$ denotes the unit leakage current, $N_F$ the total number of flip-flops, $S$ the total inverter size and $S_F$ the gate size of one flip-flop. Since our methodology does not change the gate sizes in the mapped design, the leakage power remains largely unaffected and so we concentrate on the dynamic power dissipation alone.

Table (XIV) gives the results on running stages 4-6 in our overall flow along with the improvements from stage 3 (as reported in Table (XIII)). The data shows that the iterations of stage 4-6 can reduce tapping wirelength by 37%-52% with only 1.3%-4.06% penalty on signal wirelength increase. In fact, the total wirelength is reduced by 2.6%-6.0%. After the iterations of stage 4-6, the average distance has reduced to the range of $100 - 200\mu m$, which is significantly smaller than the stub length limit indicated in [10]. The CPU time is reported at the rightmost column of Table (XIV). As one can see, most of run time is dominated by the placer. Our method converges within five iterations for all these circuits.

Table (XV) presents the results for maximum load capacitance for the network flow and ILP formulations. We compare the AFD, maximum cap and total signal wirelength of the two techniques. We observe that ILP based formulation reduces the maximum load capacitance by 25.7%-48.33%. However it increases the AFD (by 11.32%-30.82%) and total wire length (by 0.15% -7.09%). This is expected since the formulations target different objective. Hence the designer can choose between the two formulations depending upon the optimization objective. The run time for the ILP is low as explained in section (F) (Table (XI)) and repeated here for the sake of completeness.

Table (XVI) gives the power dissipation results (in $mW$) for network flow and the ILP formulations. The results (clock, signal and total power) are then compared with those obtained for the base case (shown in Table (XIII)) and the percentage

Table XIII. Experimental results for the base case, wirelength in $\mu m$, power in $mW$.

| | AFD | Tap. WL | Signal WL | Tot. WL | Clock Power | Signal Power | Tot. Power | CPU(s) |
|---|---|---|---|---|---|---|---|---|
| s9234 | 285.6 | 38550 | 244485 | 283035 | 5.06 | 6.72 | 11.78 | 70 |
| s5378 | 194.1 | 31839 | 260931 | 292770 | 4.67 | 6.84 | 11.51 | 158.1 |
| s15850 | 266.6 | 150907 | 643336 | 794243 | 20.16 | 18.07 | 38.23 | 399 |
| s38417 | 383.5 | 559586 | 1634920 | 2194506 | 68.8 | 48.35 | 117.15 | 410 |
| s35932 | 340.8 | 588823 | 1735820 | 2324643 | 74.17 | 57.88 | 132.05 | 423 |

Table XIV. Experimental results for network flow based optimization, wirelength in $\mu m$.

| Circuit | AFD | Tap. WL Final | Tap. WL Imp | Signal WL Final | Signal WL Imp | Tot. WL Final | Tot. WL Imp | CPU(s) Stg 2-5 | CPU(s) mPL |
|---|---|---|---|---|---|---|---|---|---|
| s9234 | 136.3 | 18395 | 52.28% | 247797 | -1.35% | 266192 | 5.95% | 59 | 283 |
| s5378 | 124.51 | 20419 | 35.87% | 263878 | -1.13% | 284297 | 2.89% | 25 | 439 |
| s15850 | 168 | 95136 | 36.96% | 664534 | -3.3% | 759670 | 4.35% | 186 | 995 |
| s38417 | 222.9 | 326136 | 41.72% | 1701352 | -4.0% | 202744 | 7.61% | 192 | 930 |
| s35932 | 223.12 | 385555 | 34.52% | 1799431 | -3.67% | 2184986 | 6.0% | 195 | 1153 |

Table XV. Comparison of network flow and ILP formulations, cap in $pF$.

| | Network Flow | ILP Formation | | | | | | |
|---|---|---|---|---|---|---|---|---|
| Circuit | Cap | AFD | Imp | Cap | Imp | Tot. WL | Imp | CPU(s) |
| s9234 | 0.49 | 178.25 | -30.82% | 0.33 | 32.65% | 273633 | -2.8% | 0.25 |
| s5378 | 0.39 | 138.6 | -11.32% | 0.29 | 25.64% | 284297 | -0.15% | 0.31 |
| s15850 | 1.23 | 205.8 | -22.5% | 0.70 | 43.1% | 759670 | -1.94% | 2.0 |
| s38417 | 2.52 | 274.2 | -23.0% | 1.34 | 46.83% | 2027488 | -6.59% | 6.10 |
| s35932 | 1.8 | 276.54 | 23.9% | 0.93 | 48.33% | 1927039 | -7.09% | 13.1 |

Table XVI. Power dissipation results ($mW$) for network flow and ILP formulations.

| | Network Flow Formulation | | | | | | ILP Formation | | | | | |
|---|---|---|---|---|---|---|---|---|---|---|---|---|
| Circuit | Clock | Imp | Signal | Imp | Total | Imp | Clock | Imp | Signal | Imp | Total | Imp |
| s9234 | 3.08 | 39.13% | 6.78 | -0.89% | 9.86 | 16.3% | 3.63 | 28.26% | 6.81 | -1.34% | 10.44 | 11.38% |
| s5378 | 3.55 | 23.98% | 6.89 | -0.73% | 10.44 | 9.3% | 3.79 | 18.84% | 6.84 | 0% | 10.63 | 7.65% |
| s15850 | 14.67 | 27.23% | 18.45 | -2.1% | 33.12 | 13.37% | 16.77 | 16.82% | 18.06 | 0.06% | 34.83 | 8.89% |
| s38417 | 45.82 | 33.4% | 49.56 | -2.5% | 95.38 | 18.58% | 53.21 | 22.66% | 48.19 | 0.33% | 101.4 | 13.44% |
| s35932 | 54.15 | 26.99% | 59.05 | -2.02% | 113.2 | 14.27% | 63.24 | 14.74% | 52.64 | 9.05% | 115.88 | 12.25% |
| Ave | 29.55 | 30.15% | 28.15 | -1.65% | 52.4 | 14.36% | 28.13 | 20.26% | 26.51 | 1.62% | 54.64 | 10.72% |

Table XVII. Wirelength capacitance product comparison.

| Circuit | Network Flow, WCP | ILP Formation, WCP | Imp |
|---|---|---|---|
| s9234 | 130434 | 90298.9 | 30.77% |
| s5378 | 110717.6 | 82446.1 | 25.53% |
| s15850 | 934394.1 | 542083.5 | 41.99% |
| s38417 | 5109269.8 | 2895290.9 | 43.32% |
| s35932 | 3238975.8 | 1792146.3 | 44.67% |

improvement is also reported. The network flow algorithm gives an average power improvement of 14.36% whereas the corresponding improvement for the ILP formulation is 10.72%. This is expected since the network flow algorithm tries to minimize the total tapping length which in-turn minimizes the clock net length and the power dissipation. It may be noted that the trend in power dissipation follows that of wirelength reduction for both clock and signal nets (as expected).

It is often difficult to compare two techniques that have different optimization objectives. In such cases, it is better to come up with one objective that can be used for comparison. A classic example of such a case is the Power-Delay-Product (PDP). In circuit optimization (especially gate-sizing), one could trade-off power for delay improvement and vice-versa. Hence PDP is used a metric to compare different techniques. In our methodology we trade-off wirelength and maximum load capacitance and hence we introduce the metric Wirelength-Capacitance-Product (WCP). This has obvious parallels with the PDP since wire length is directly related to power dissipation and maximum load capacitance is related to delay. Table (XVII) presents the results for both the techniques in terms of WCP. WCP is reported in $\mu m\ pF$. It may be observed that the ILP formulation results in much better WCP.

CHAPTER V

COMBINATORIAL ALGORITHMS FOR FAST CLOCK MESH OPTIMIZATION

We present fast and efficient combinatorial algorithms for clock mesh optimization. Our contributions in this work are two-fold. We first present a set-cover based formulation that performs simultaneous mesh buffer placement and sizing. We also present mesh reduction algorithms that trade off skew tolerance for low power dissipation. This algorithm gives a framework for the designer to choose the desired trade off point (between circuit delay and power dissipation).

A.  Preliminaries

We shall introduce certain notations and conventions which will be followed throughout this chapter.

- $m \times n$ denotes the dimension of the clock mesh. $I$ denotes the set of nodes in the mesh.

- Clock buffers of $B$ sizes $\{b_1, b_2, \ldots b_k\}$ in non-decreasing order. Buffer $b_i$ can drive a load of capacitance at most $c_i$.

- *Buffer Mapping Function $BM : i \to j$* maps each node location $i \in I$ to $j \in B$. $BM(i) = \phi$ implies that the location $i$ has no buffer in it.

- $S = \{s_1, s_2 \ldots s_c \}$ denotes the set of clock sinks. Without loss of generality, we assume that each sink $s_i$ is connected to node $i \in I$ (in reality, the clock sinks will be connected to the closest point in the mesh which need not be in the intersection of the horizontal and vertical grid lines). The node $i$ in the mesh is referred to as the *connection node* of sink $s_i$. $d_{ij}$ denotes the minimum distance

between node $i$ and $j$ in the mesh.

- $T_{clock}$, $t_{hold}$ and $t_{setup}$ denote the clock period, hold time and set up time respectively.

- The maximum permissible delay of logic network between any two registers $(i, j)$ is given by [1]:

$$P_{delay}^{ij} = T_{clock} - t_{setup} - skew_{ij} \tag{5.1}$$

- $P_{delay} = min_{\forall(i,j)}P_{delay}^{ij}$ denotes the maximum permissible delay of the entire circuit.
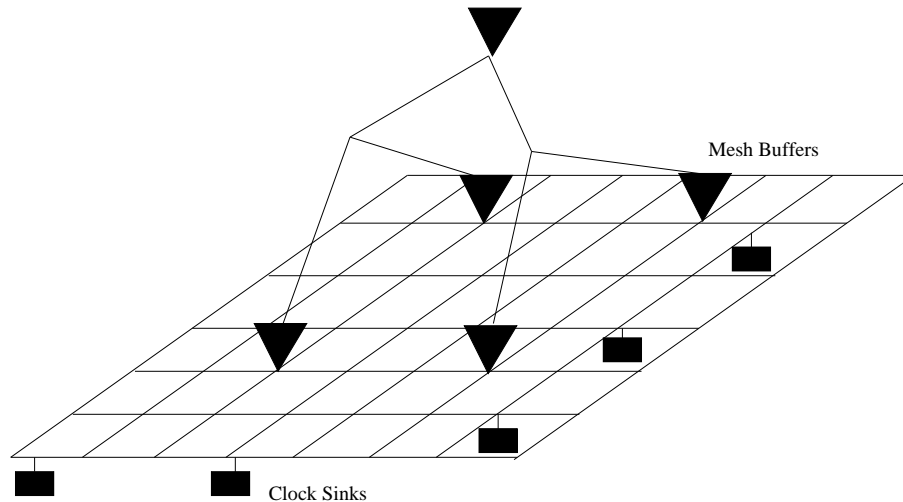
B.   Previous Work



Fig. 17. Mesh driven by a top level tree.

One of the most widely used non-tree based CDN is clock mesh. Figure (17) shows a typical clock mesh [55, 50, 25]. The mesh consists of a rectangular grid

driven by a top level tree. The buffers at the leaf of the top level tree shall henceforth be referred to as **mesh buffers**. The clock sinks or subnetworks are connected to the closest point in the mesh. Since there are several paths between the source and the clock sinks, there is a high level of redundancy and this redundancy translates to high tolerance to variations in clock skew. Mesh architecture is used mainly in high performance systems. In fact, it has been used in commercial microprocessors such as IBM G5 [11], Power4 [12] and SUN Sparc V9 [13]. In all the above processors, a very low clock skew has been reported which proves the effectiveness of the clock mesh in mitigating skew variability.

The skew tolerance in mesh based architecture does not come for free. Clock mesh consumes significantly higher wire area compared to tree based distributions. In fact, a hybrid mesh architecture could consume up to 168% higher area compared to tree [56]. Higher wire area leads that a higher load capacitance for the clock buffers which in turn implies a higher power dissipation. There is an increasing demand to deliver devices with higher battery life - even at the expense of lower operating frequency. It is possible that future designs may trade off frequency for lower power dissipation.

The maximum permissible delay of logic network between any two registers $(i, j)$ is given by Equation (5.1). The maximum permissible delay is a more direct metric to evaluate circuit characteristic than clock skew. Skew becomes important when it affects circuit delay (for example, in non-zero skew design, skew could be made intentionally to deviate from zero to meet the delay specifications). Typically, in the zero skew design $skew_{ij}$ is designed to be zero. However, this may increase due to variations subsequently reducing the maximum speed at which the circuit can function. Higher skew would bring down the maximum permissible delay $P_{delay}$. Hence a mesh architecture is suited well for high performance systems since it mitigates the

variations in clock skew even though the resource consumption is high (wire length, power etc.). With power occupying an increasingly important role in chip design, it is necessary to find the most desirable skew-power trade off. At the very least, the designer should be given the flexibility to do so. For CDN design, this could imply a higher skew for lower power dissipation. Since a significant portion of the total power consumption comes from the clock network (up to **40%** of the total power dissipated in high performance systems [57]) and clock mesh consumes a high area/power overhead, there is a need to address more efficient ways of designing/optimizing the clock mesh. Even though there has been previous works on in mesh architecture, the following issues remain largely unaddressed:

- What are the ideal locations for the mesh buffers to drive the clock mesh? Is it ok to distribute the mesh buffers uniformly across the mesh?

- Can the mesh buffers be sized differently? If yes, then does it work better than sizing uniformly?

- A mesh has a high level of redundancy. Can some amount of redundancy be sacrificed to reduce the wire length? If yes, then how much is the trade-off? Can we quantify the skew vs power trade-off?

In this work, we address all the above mentioned issues. Our contributions include:

- We propose a set-cover based algorithm for finding the mesh buffer locations and their sizes. Our algorithm works fast on a discrete library of buffer sizes. We show that such a buffer placement and sizing yields better results compared to uniform sizing.

- We formulate the mesh reduction problem by using survivable network theory. We present heuristics for solving the formulation efficiently. Experimental

results indicate up to **29% reduction in wire length, 28% reduction in power with less than 3.3% increase in delay penalty.**

- Our techniques allow the designer to trade-off between skew and power dissipation. In fact, the formulation presented is flexible enough to allow a high range of trade-off (that is either a high skew- low power design or a low skew - high power design or anywhere in between).

- Our algorithms run very fast. It can process test cases with over a thousand sinks within a few seconds. Such a high speed helps the designer to run the same algorithm several times with different parameter values that produce different solutions in the power delay curve.

## C.  Problem Statement

**Simultaneous Mesh Buffer Placement and Sizing**

*Find the function BM or for each candidate buffer location (there are $m \cdot n$ such locations), find (a) If a buffer is required and (b) The size of buffer needed such that the following constraints are satisfied: (i) Each node in the mesh is allocated to at least one buffer, (ii) Each buffer drives less than the maximum load it can drive, and (iii) The total sum of the buffer sizes is minimized.*

**Mesh Reduction**

*Remove edges from the mesh such that (i) Each sink $s_i$ has at least $k$ node locations such that for each such node location $j$, $d_{ij} \leq L_{max}$, $BM(j) \neq \phi$ and there exists at least $l$ edge disjoint paths between $j$ and $i$, (ii) The number of edges removed is maximized. $k$, $L_{max}$ and $l$ are user defined constants.*

The mesh reduction problem attempts to remove edges such that there exists at least certain number of buffers that connect each clock sink with short paths. The user

defined parameters control impact the solution in the following manner: Setting $k$ and $l$ high would mean more redundancy and hence more tolerance to variations but less number of edges removed or more power dissipation. By varying the parameters $k$ and $l$, the designer has the flexibility to trade variation tolerance to power dissipation. The restriction $L_{max}$ helps in restricting the delay between the mesh buffers and the clock sinks. This in turn, helps in keeping the skew low.

The buffers are sized with the assumption that they are driving a complete mesh. After mesh reduction, the buffers could be driving a load that is significantly lesser than that of a complete mesh. Hence, as a post-processing step, we compute the new load and down-size the buffers accordingly. This procedure (as indicated in Figure 18) will be detailed in this chapter.

D. Simultaneous Mesh Buffer Placement and Sizing via Set Cover

1. Algorithm Description

The **Set Cover** problem can be stated as follows: Given a set universe $\mathcal{U}$ and a collection $\mathcal{S}$ of subsets of $\mathcal{U}$, find a minimum size subset $\mathcal{C} \subset \mathcal{S}$ such that $\mathcal{C}$ covers $\mathcal{U}$. The above definition can be modified to weighted set cover problem by assigning weights of each set in $\mathcal{S}$. In this section, we shall show that the mesh buffer placement/sizing problem can be formulated as an instance of the set cover problem.

For each node in the mesh, define a **Covering Region** as follows. Covering Region of the node for a particular buffer is defined as the set of nodes around the node in the 2-dimensional mesh such that the total capacitance of the nodes included in the covering region (including the mesh capacitance as well as the nodes that the mesh drives) is less than the maximum capacitance that the buffer can drive. Figure (19) depicts the covering region of a buffer placed at a point in a 2-dimensional
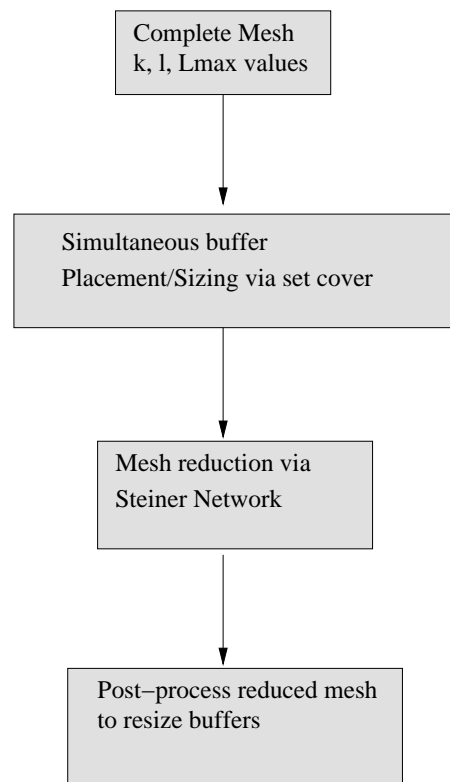
Fig. 18. Overall flow for mesh buffer sizing and reduction.

mesh grid. The dashed lines indicate the regions of the mesh that can be driven by the buffer without violating the maximum load constraint of the buffer. If any more edges in the mesh are added, then the capacitance of the region will be greater than the maximum load that the buffer can drive. Let $CR_i^j$ denote the covering region of node $i \in I$ while driven by buffer $j \in B$. That is $CR_i^j \in I$ for each $i \in I$ and $j \in B$. Let $SCR$ denote the super set of covering regions. We can draw the parallels between the above defined variables and the instance of set cover defined earlier:

- The set of $I$ of node locations can be considered as the universe $\mathcal{U}$.

- The covering regions $CR_i^j$ form the collection of subsets $\mathcal{S}$.

- If the buffer size $b_j$ denotes the weight of a subset $CR_i^j$, then the objective is to "pick" minimum weighted sum of subsets such that each node has at least one subset covering it.

In other words, the mesh buffering problem is identical to the set cover problem with $I \Leftrightarrow \mathcal{U}$ and $SCR \Leftrightarrow \mathcal{C}$. **If $CR_i^j$ is picked, then node $i \in I$ is driven by buffer $j \in B$.** For example, consider a 2x2 mesh whose nodes are numbered $\{0, 1, 2, 3\}$. Let the number of buffer types be 2 namely $(a, b)$. The number of subsets would then be 8. Let the subsets be numbered $(a_0, a_1, a_2, a_3, b_0, b_1, b_2, b_3)$. If the solution picks subset $a_0$, then node "0" of the mesh will be driven by buffer type "$a$".

To motivate the solution approach, we shall now state the same problem in mathematical terms using indicator variables. Let $x_i^j$ denote the indicator variable that is set to 1 if $CR_i^j$ is picked in the solution. Then the problem can be stated as:

$$\text{minimize} \sum_{j \in B} \sum_{i \in I} b_j x_i^j \qquad (5.2)$$
$$\cup_{(i,j):x_i^j=1} CR_i^j \supseteq I$$

Dashed lines indicate covering region of the buffer shown
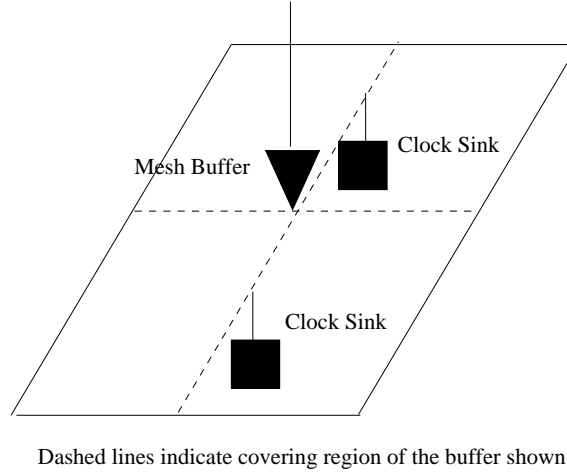
Fig. 19. Example of covering region.

Note that irrespective of the approach towards solving the set cover problem, it is possible that the algorithm may return two buffers for the same location, which is not a feasible solution. However such a situation can be easily avoided by using the observation and lemma stated below.

**Observation 1:** For any node $i \in S$, $CR_i^j \supseteq CR_i^l$ if $b_j > b_l$. The observation comes from the fact that a bigger buffer size can drive a bigger load.

**Lemma 1:** In any optimal solution $\Phi$, for any node $i$, there can be at most one buffer $j$ such that $x_i^j = 1$.

**Proof:** Direct consequence of *Observation 1*. If there exists two buffers $j$ and $l$ such that $x_i^j = 1$ and $x_i^l = 1$ and $b_j \geq b_l$, then $CR_i^l$ can be removed from $\Phi$ without loss of feasibility. This implies that $\Phi$ is not optimal and hence a contradiction.

**Corollary 1:** In any solution $\Phi$, for any node $i$, if there are more than one buffer driving a node, one can pick the biggest buffer without losing feasibility.

At the end of algorithm, the solution is pruned using Corollary 1.

Although there are several ways to implement the set cover algorithm, we shall

implement it using the greedy algorithm. The greedy algorithm can be stated as follows: *Pick the set that covers the most nodes and then throw away the nodes that are covered. Repeat this process until all nodes are covered.* The greedy algorithm is simple, yet has a proven approximation guarantee. If $OPT$ is the value of the optimal solution and $|\mathcal{U}|$ is the size of the universe $\mathcal{U}$, then it can be shown that the greedy algorithm produces a solution of size at most $OPT(ln(\frac{|\mathcal{U}|}{OPT}) + 1)$ [51]. This essentially proves that greedy algorithm has an approximation guarantee of $O(ln(|\mathcal{U}|))$. Inapproximability results show that this is the *best* approximation guarantee that any algorithm can produce for the set cover problem [58]. The algorithm is detailed in Figure (20). Notice that we have modified the algorithm slightly to take care of set weights (in this case the buffer sizes). As it will be detailed in the experimental section, the set cover implementation runs very fast in practice (within few seconds a test case with more than 1700 sinks).

## 2. Complexity Analysis and Near-Continuous Sizing

In this section, we present the complexity analysis and show how our algorithm can be extended to continuous sizing (in practice). Let $\alpha$ denotes the minimum size of a subset. In other words, $\alpha$ denotes the minimum number of nodes in the mesh covered by the minimum buffer size in the library. Let $N$ denotes the number of nodes in the mesh and $\beta$ the size of the buffer library. Since each iteration of the algorithm (in Figure (20)) covers at least $\alpha$ nodes, it is easy to see that the complexity of the algorithm is $O(\frac{N\beta}{\alpha})$. Essentially, the algorithm is linear with the mesh size and number of buffer types. Figure (2) shows the plot of CPU time verses the number of buffer types for the test case s35932. The figure illustrates the following aspects of our buffer placement/sizing algorithm:

1. The run time increases linearly with number of buffer types.

2. We ran the experiment with 41 buffer types. The minimum and maximum buffer sizes were set to 20x and 60x times that of a minimum size inverter. In other words, we had a buffer size granularity equal to the size of a minimum inverter. Our set up is equivalent to *near continuous sizing*. Even in such a scenario, the run time of our algorithm (as indicated in Figure (2)) was about half a minute. Hence we can conclude that our algorithm is expendable for large library sizes as well as continuous sizing - if necessary.

| Greedy set cover for mesh buffer placement/sizing. |
|---|
| Input : $SCR = \cup\, CR_i^j$ for each $i \in I$ and $j \in B$ |
| Output : $M$ = set of covering regions that are picked |
| 1. $M \leftarrow \phi$<br><br>2. While $M$ does not cover $I$ do<br><br>    2.1 For each unpicked covering region $CR_i^j$<br><br>       define $C_{eff} = \frac{b_j}{\|CR_i^j - M\|}$<br><br>    2.2 Pick set $C$ with least $C_{eff}$.<br><br>    2.3 $M \leftarrow M \cup C$<br><br>3. For each node $i \in I$, if there exists $j \in B$ and $l \in B$<br><br>    both $CR_i^j$ and $CR_i^l$ are picked and $b_j > b_l$<br><br>    drop $CR_i^l$ from the solution. |

Fig. 20. Greedy set cover for mesh buffer placement/sizing.
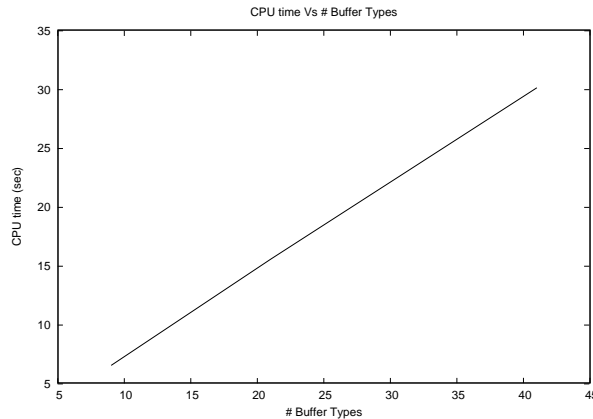
Fig. 21. CPU time vs # buffer types for s35932.

E.   Mesh Reduction and Post-Processing

### 1.   Mesh Reduction

Once we locate the position of the mesh buffers and their sizes (from the buffer library), the next task is to reduce the size of the mesh. This is done by removing edges such that a certain level of redundancy is still maintained. The exact definition of the problem was stated in section (C).

We propose to solve the mesh reduction problem using similar solutions used in the design of robust communication networks. The communication networks are prone to frequent failures. Survivability makes the network functional even in the presence of link failures. This is often done by creating redundant paths that are edge disjoint (thereby increasing the chances of at least one path being active in the presence of failures). This concept has striking parallels to the clock mesh which is designed with redundancy to account for tolerance to variations. The *Steiner Network Problem* and its variants have been used in the design of survivable networks. In its generalized form the Steiner Network problem can be stated as follows:

*Given (a) Graph $G = (V, E)$ (b) A cost function c for the edges and (c) A connectivity requirement function $r : V^2 \to Z^+$, find a minimum cost subgraph in $G$ such that there exists at least $r(u, v)$ edge disjoint paths for every ordered pair $u, v \in V$.*

Notice that one may set $r(u, v) = 0$ for those vertex pairs that do not have a connectivity requirement. One could also set an upper bound on the number of time an edge is used in the network. The Steiner Network problem generalizes the Steiner Forest problem which in turn generalizes the Steiner tree problem. Hence it is NP-Hard. Interested reader may refer to [51, 59, 60] for details about the Steiner network problem and survivable networks. We shall abstract the problem of mesh reduction into Steiner Network problem.

Three parameters: $k$, $l$ and $L_{max}$ define an instance of the mesh reduction problem (please refer to section (C) for definition of the parameters). For the sake of simplicity, we shall first assume that there is no constraint on $L_{max}$ or path length. We shall later show that the constraint is taken care of implicitly in our formulation. We transform the mesh reduction problem into Steiner Network by the following procedure:

1. Let the mesh be represented by a graph $G = (V, E)$.

2. Set connectivity requirement function $r(u, v) = 0$ for all $(u, v) \in V$.

3. For each clock sink $s_i \in S$, identify $k$ closest mesh buffer locations (say) $T_i = (t_1, t_2, \ldots t_k)$.

4. Set $r(i, j) = l$ for all $s_i \in S$ and $T_i$.

Figure (22) gives a simple example that illustrates the concept of mesh reduction. Let the parameters be set to the following values: $k = 1$, $l = 2$ and $L_{max} = 3$. This implies that for each clock sink there must be at least one buffer at a distance less

than or equal to 3 and there must be at least 2 edge disjoint paths between this buffer and the clock sinks. It is easy to see that such a requirement is satisfied even after removing the edges indicated with dashed lines in Figure (22).
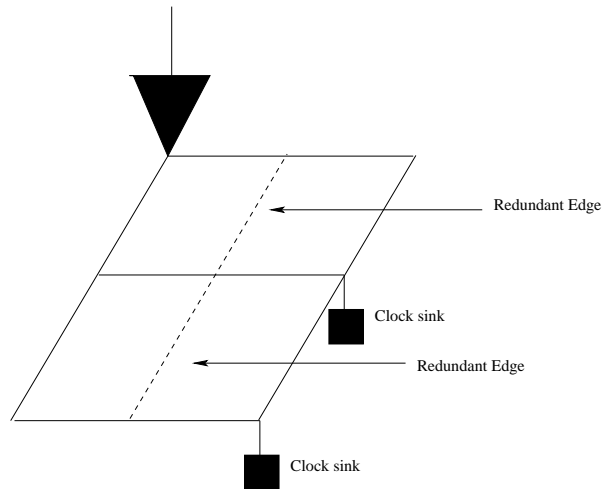


Fig. 22. Simple example for mesh reduction.

Now, one may use any Steiner Network Optimization algorithm (like [59]) on the above instance. Since we identify the $k$ closest buffers in the connectivity requirement, the short path constraint (by means of $L_{max}$) is implicitly taken care of. This is due the fact that if these closest buffers do not satisfy the $L_{max}$ requirement, it is easy to see that there exists no other buffer locations than can satisfy the constraint and $L_{max}$ requirement should be relaxed. Further, because of the connectivity requirement, edges in the shortest pairs will be retained. To solve the Steiner Network problem, we use a simple greedy heuristic. Other complicated approaches like LP-rounding [59] or path length constrained network approaches [61] can also be used. But we found that the one detailed above produces good results with a very low run-time.

An overview of our algorithm for Steiner Network minimization is shown in Figure (23). The algorithm starts with initializing the cost of all edges to unity.

This is followed by identifying edge disjoint paths between clock sinks and the closest $k$ mesh buffers. It is worthy to mention three points about identifying these paths: (a) The disjoint path requirement is between a clock sink and a *particular* mesh buffer and not across all the $k$ assigned buffers. For example, if a sink $a$ is assigned to buffers at locations $b$ and $c$, then we need to identify $l$ disjoint paths between $a$ to $b$ (say $P_{ab}$) and $a$ to $c$ (say $P_{ac}$). While the paths within $P_{ab}$ and $P_{ac}$ are edge disjoint, they are allowed to share edges across each other. (b) Since it is cost driven, the cost of an added edge is set to zero and the algorithm tries to maximize the usage of edges which improves the quality of the solution and (c) Since the mesh graph has a very regular structure (planar grid), it is easy to identify the paths. Also, we would like to point out that our algorithm is **tailor made** for the problem in hand and hence works fast. It may not produce good results on general graphs. In essence, this should be treated as a heuristic that exploits our specific problem structure. Experimental results indicate that our algorithm runs **very fast** achieving run-time within **few seconds** even for a test case with more than 1,700 sinks.

## 2. Post-Processing for Mesh Reduction

The buffers are placed and sized with the assumption that they are driving a complete mesh. However, this may not be the case after mesh reduction. Hence there is a potential to reduce the size of the buffers after mesh reduction. In post-processing, we find the new capacitance of the covering regions and under-size the buffers if necessary. Let:

- $R$ denote the set of edges that were removed from the mesh.

- $cap(e)$ denote the capacitance of edge $e$.

- $cap(CR_i^j)$ denote the capacitance of a covering region. This capacitance includes

| Greedy Steiner Network for Mesh Reduction |
|---|
| Input : $G = (V, E)$, and connectivity requirements |
| Output : $E' \subset E$ satisfies connectivity requirements |
| 1. For each $e \in E$, set $c(e) = 1$. <br><br> 2. Initialize $E' \leftarrow \phi$ <br><br> 3. For each sink $s_i \in S$ <br><br>      3.1 Find $k$ closest buffers locations <br><br>      3.2 Identify $l$ minimum cost disjoint paths <br><br>         (denoted by $P_i$) between $s_i$ and <br><br>         identified buffer locations <br><br>      3.3 For each $e \in P_i$, <br><br>       3.3.1 $E' \leftarrow E' \cup e$, $c(e) = 0$. <br><br> 4. Output $E'$. |

Fig. 23. Greedy mesh reduction.

| Post processing of buffer sizes after mesh reduction |
|---|
| Input : Mesh buffer sizes and reduced mesh |
| Output : New buffer sizes for the reduces mesh |
| 1. For each $i \in I$ (set of buffer nodes) with $b_i > 0$<br>    1.1 Find minimum buffer size (say $b_k$) that can<br>        drive $cap_r(CR_i^j)$.<br>    1.2 If $b_k < b_i$, $b_i \leftarrow b_k$ |

Fig. 24. Post processing after mesh reduction.

capacitance of the mesh edges as well as the input capacitance of the clock sinks.

- $cap_r(CR_i^j)$ denote the capacitance of the covering region in the *reduced mesh*. $cap_r(CR_i^j)$ is computed using:

$$cap_r(CR_i^j) = cap(CR_i^j) - \sum_{e \in R, e \in CR_i^j} cap(e) \qquad (5.3)$$

- $b_i$ denote the size of the buffer at node $i$.

Figure (24) gives the description of the post processing algorithm. We first compute the capacitance of the covering regions after accounting for the deleted edges. Each buffer in the library is characterized by the maximum capacitance that it can drive. If a certain node in a mesh has a buffer assigned to it, we then assign the minimum size buffer in the library than can drive the capacitance of the covering region - after accounting for the removed edges.

Table XVIII. Benchmark characteristics.

| Case | #Sinks | Mesh Size | (LxW) ($\mu m$) |
|---|---|---|---|
| s9234 | 135 | 9x9 | 1710x1644 |
| s5378 | 165 | 10x10 | 1629x1600 |
| s13207 | 500 | 30x30 | 2523x2592 |
| s15850 | 566 | 30x30 | 2769x2720 |
| s38584 | 1426 | 40x40 | 4626x4672 |
| s35932 | 1728 | 40x40 | 5321x5376 |

F.   Experimental Results

1.   Experiment Set up

The algorithms were implemented in C++ and simulations were run on a Linux Work Station with 2GB RAM. The proposed techniques were verified using experiments performed on the ISCAS89 benchmark circuits. The characteristics of the ISCAS89 circuits are shown in Table (XVIII). The ISCAS89 benchmark suites were synthesized using SIS [41] and placed using mPL [42]. The table indicates the number of sinks, mesh size and chip dimensions. All HSPICE simulations were done using $65nm$ process model cards from BPTM [40]. The interconnect parameters were obtained from [39]. The following notations will be used in the tables presented:

- **WL** denotes the wire length ($\mu m$).

- $skew_{nom}$ denotes the nominal skew (measured when parameters are set to ideal values) and $\mu_{skew}$ ($\sigma_{skew}$) denotes the mean (standard deviation) of the skew due to variations. $skew_{max}$ equals $\mu_{skew} + 3\sigma_{skew}$. All skew measurements are presented in $psec$.

- **Pow** denotes power dissipation measured in $mW$. The power dissipation is measured using HSPICE simulations that measure the current drawn by the devices in an entire clock cycle and computing the area under the voltage vs. current curve. Hence this power includes both dynamic, leakage and crow-bar power dissipation.

- **SV (Slew Violation)** is the maximum positive deviation at all the clock sink locations from the user specified value. That is if $slew_r$ denotes the required slew and $slew_{max}$ denotes the maximum slew among the sink nodes, then:

$$\text{SV} = 100 * \frac{(slew_{max} - slew_r)}{slew_r} \tag{5.4}$$

If the slew violation is negative, then it is set to zero. The $slew_r$ is set to $150psec$.

- $P_{delay}$ measures the maximum permissible delay as defined by equation (5.1). $P_{delay}$ measurements are presented in $psec$.

## 2.   Experiment Design

In this work, we propose the following techniques:

1. Simultaneous mesh buffer placement/sizing.

2. Mesh reduction.

In order to measure the effectiveness of the above mentioned techniques, we conducted the following experiments:

- Compare our mesh buffer placement/sizing algorithm with uniform sizing. By uniform sizing, we mean placing buffer of single size uniformly distributed

throughout the mesh. We do the experiments for small, medium and large buffer sizes from the library.

- Compare our mesh reduction with that of complete mesh.

We make comparisons in terms of wire length, power dissipation, nominal skew and variation skew. For measuring the impact of variation on clock skew, we constructed a zero skew buffered clock tree to drive the clock mesh. The clock tree construction follows the techniques presented in [31].

For Monte Carlo simulations, the following parameters were varied (a) buffer channel length (b) interconnect wire width (c) VDD and (d) sink load capacitance. The above parameters are varied with mean as the nominal value and the $\sigma$ value set to 5% of the nominal value. Spatial correlation among all the variations was accounted by using the Principal Component Analysis [29]. The Monte Carlo simulations were done using HSPICE.

## 3.   Results

The results for our mesh simultaneous buffer placement/sizing algorithm (henceforth referred to as *sizing algorithm*) is shown in Table (XIX). The second, third and fourth columns indicate the total buffer area, wire length and power dissipation respectively. Buffer area is reported in terms of the buffer area of a minimum size inverter (that is, if the buffer area is 100, then the actual buffer area is 100x times the active area of a minimum size inverter). In the next column, we report the nominal skew. This is followed by a set of three columns that denote mean, standard deviation and maximum skew due to variations (obtained by running 1000 Monte Carlo simulations). The last three columns denote the Slew Violation (computed using Equation (5.4)), maximum permissible delay and CPU time respectively. $P_{delay}$ is computed by subtracting the

clock period (assuming 1GHz clock) with $skew_{max}$. The following conclusions can be drawn from Table (XIX).

- Our sizing algorithm meets the slew specifications (within **2.5%** on an average).

- The run time of our algorithm is within a few seconds and is therefore largely inconsequential.

We compare our approach with the one where identical buffers were placed at symmetric nodes in the mesh. Tables (XX), (XXI) and (XXII) present the nominal, variation skew area, power and $P_{delay}$ values when the smallest, medium size and largest buffer sizes are used to drive the mesh at symmetric nodes respectively. The tables also provide the ratio comparison (of area, power and $P_{delay}$) between uniform sizing and our sizing algorithm (results in Table (XIX)). It is worth noting that the skew results (both nominal and variation) from our sizing algorithm is not very different (within $15psec$) from the ones obtained by using uniform sizing. The following inferences can be made:

- Using the smallest buffer uniformly results in an area reduction of 37% compared to our sizing algorithm. However, it also leads to 33% slew violation on an average and up to 77% in some cases. $P_{delay}$ values are identical for almost all the approaches.

- Medium buffer sizes satisfy slew constraints in all but one case and large buffer size satisfies the slew constraints in all the cases. But, this comes at an area penalty of 21% (46%) for medium (large) buffer size.

Figures (25,26,27) gives the worst case output signal (signal at the sink that has the worst slew) while using small, medium, large buffer sizes. Figure (28) gives the

Table XIX. Results for the buffer placement/sizing algorithm.

| Case | Area | WL | Pow | $skew_{nom}$ | $\mu_{skew}$ | $\sigma_{skew}$ | $skew_{max}$ | SV | $P_{delay}$ | CPU |
|---|---|---|---|---|---|---|---|---|---|---|
| | | ($\mu m$) | (mW) | (ps) | (ps) | (ps) | (ps) | (%) | (ps) | (sec.) |
| s9234 | 1140 | 30366 | 7.8 | 33.0 | 37.2 | 6.3 | 56.1 | 6.4 | 943.9 | 0.1 |
| s5378 | 1350 | 32290 | 8.4 | 29.1 | 44.0 | 5.5 | 60.1 | 0.0 | 939.5 | 0.1 |
| s13207 | 4870 | 153450 | 31.3 | 22.9 | 46.9 | 17.0 | 97.8 | 0.0 | 902.2 | 0.7 |
| s15850 | 5370 | 164670 | 34.2 | 21.8 | 31.4 | 10.0 | 61.4 | 0.0 | 938.6 | 0.7 |
| s38584 | 11410 | 371900 | 80.2 | 33.0 | 66.1 | 14.8 | 110.6 | 1.0 | 889.4 | 4.3 |
| s35932 | 12660 | 427900 | 94.9 | 36.2 | 65.4 | 11.6 | 100.0 | 7.7 | 900.0 | 4.7 |
| Ave | 6135 | 196763 | 42.8 | 29.3 | 48.5 | 10.9 | 81.1 | 2.5 | 918.9 | 1.8 |

Table XX. Results for uniform sizing - smallest size.

| Case | Smallest Buffer | | | | | | | | | | |
|------|------------------|------------|------------------|------------------|--------|------|-------|------|-------|------------|-------|
|      | $skew_{nom}$ | $\mu_{skew}$ | $\sigma_{skew}$ | $skew_{max}$ | SV (%) | Area | Ratio | Pow | Ratio | $P_{delay}$ | Ratio |
| s9234 | 31.5 | 29.6 | 7.8 | 53.0 | 25.00 | 980 | 0.86 | 7.9 | 1.01 | 947.0 | 1.00 |
| s5378 | 19.6 | 23.6 | 3.2 | 33.2 | 17.20 | 999 | 0.74 | 8.1 | 0.96 | 966.8 | 1.03 |
| s13207 | 16.3 | 34.1 | 9.9 | 63.8 | 10.55 | 3847 | 0.79 | 31.4 | 1.00 | 936.2 | 1.04 |
| s15850 | 16.4 | 32.9 | 12.5 | 70.3 | 18.54 | 3866 | 0.72 | 33.9 | 0.99 | 929.7 | 0.99 |
| s38584 | 36.0 | 63.8 | 15.1 | 109.0 | 47.49 | 7531 | 0.66 | 78.8 | 0.98 | 891.0 | 1.00 |
| s35932 | 50.7 | 69.4 | 10.3 | 100.4 | 77.05 | 7723 | 0.61 | 92.1 | 0.97 | 899.6 | 1.00 |
| Ave | 28.4 | 42.2 | 9.8 | 71.6 | 32.64 | 4158 | 0.73 | 42.03 | 0.98 | 928.4 | 1.01 |

Table XXI. Results for uniform sizing - medium buffer size.

| Case | Medium Buffer | | | | | | | | | | |
|---|---|---|---|---|---|---|---|---|---|---|---|
| | $skew_{nom}$ | $\mu_{skew}$ | $\sigma_{skew}$ | $skew_{max}$ | SV (%) | Area | Ratio | Pow | Ratio | $P_{delay}$ | Ratio |
| s9234 | 25.6 | 25.3 | 7.0 | 46.2 | 0.00 | 1642 | 1.44 | 8.4 | 1.08 | 953.8 | 1.01 |
| s5378 | 21.5 | 23.0 | 3.4 | 33.2 | 0.00 | 1661 | 1.23 | 8.7 | 1.04 | 966.8 | 1.03 |
| s13207 | 14.6 | 35.6 | 9.9 | 65.2 | 0.00 | 6380 | 1.31 | 32.7 | 1.04 | 934.8 | 1.04 |
| s15850 | 14.9 | 40.7 | 13.6 | 81.4 | 0.00 | 6390 | 1.19 | 35.2 | 1.03 | 918.6 | 0.98 |
| s38584 | 28.3 | 61.3 | 14.8 | 105.7 | 0.00 | 12551 | 1.10 | 81.5 | 1.02 | 894.4 | 1.01 |
| s35932 | 39.3 | 68.7 | 13.6 | 109.3 | 13.23 | 12787 | 1.01 | 95.3 | 1.00 | 890.7 | 0.99 |
| Ave | 24.0 | 42.4 | 10.4 | 73.5 | 2.21 | 7442 | 1.21 | 43.63 | 1.03 | 926.5 | 1.01 |

Table XXII. Results for uniform sizing - largest buffer size.

| Case | Largest Buffer | | | | | | | | | | |
|------|----------------|---|---|---|---|---|---|---|---|---|---|
| | $skew_{nom}$ | $\mu_{skew}$ | $\sigma_{skew}$ | $skew_{max}$ | SV (%) | Area | Ratio | Pow | Ratio | $P_{delay}$ | Ratio |
| s9234 | 23.2 | 24.8 | 5.9 | 42.6 | 0.00 | 1972 | 1.73 | 8.8 | 1.13 | 957.5 | 1.01 |
| s5378 | 17.7 | 21.2 | 3.2 | 30.7 | 0.00 | 1998 | 1.48 | 9.1 | 1.08 | 969.3 | 1.03 |
| s13207 | 13.0 | 38.6 | 4.2 | 51.2 | 0.00 | 7695 | 1.58 | 34.1 | 1.09 | 948.8 | 1.05 |
| s15850 | 11.9 | 44.8 | 14.6 | 88.7 | 0.00 | 7679 | 1.43 | 36.6 | 1.07 | 911.3 | 0.97 |
| s38584 | 24.7 | 62.7 | 14.8 | 107.0 | 0.00 | 15175 | 1.33 | 75.3 | 0.94 | 893.0 | 1.00 |
| s35932 | 34.9 | 69.4 | 13.7 | 110.6 | 0.00 | 15319 | 1.21 | 91.1 | 0.96 | 889.4 | 0.99 |
| Ave | 20.9 | 43.6 | 9.4 | 71.8 | 0.00 | 8955 | 1.46 | 42.50 | 1.05 | 928.2 | 1.01 |

corresponding plot while using our sizing algorithm. In each of the above mentioned plots, the ideal signal output (with signal slew of $150psec$) is also shown for comparison. The plots were obtained for the test case s35932. Notice that using large buffer type as well as using our sizing algorithm gives a waveform that closely resembles the ideal output. However, using large buffer size will result in 46% increase in buffer area. Using small and medium buffer sizes gives a signal waveform that deviates significantly from the slew specification.

Next we compare the results of the mesh reduction algorithm. We compare both resource consumption and tolerance to variation. The results are indicated in Table (XXIII). We present the wire length and power reduction when compared to the complete mesh. Table (XXIII) also presents the nominal skew, mean, standard deviation, maximum skew value and the maximum delay ($P_{delay}$) obtained on running Monte Carlo simulations run with the set up described earlier. The results can be summarized as follows:

- Mesh leads to a **wire length reduction of 25.9% and power savings of 18.5% on an average.**

- In some test cases the power savings can be as high as **28%.**

- These savings do have an impact on the tolerance to variations. However, it can be seen that the delay penalty is less than 3.3% on all the cases. In fact, the delay penalty is **less than 1%** for the two largest test cases. The nominal skew results are identical to those obtained without reduction. Hence mesh reduction preserves the nominal skew.

Figure (29) gives the power vs. maximum skew trade off curve for test case s9234. The Y-axis measures the power dissipation and X-axis measures the $skew_{max}$

value after measuring the skew using Monte Carlo simulations. Each point in the curve is obtained by setting a different value of $k$. A higher value would imply more paths, more wire length, more power dissipation, lower skew and higher $P_{delay}$ and vice-versa for lower $k$ ($k$ is the number of buffers each sink should be connected to with paths of short length as defined in section (C)). Since our algorithm is very fast, the user can potentially run it for different values of $k$ and pick the one meets the design specifications. Thus it provides a **framework for trade off** between skew and power dissipation.

Table (XXIV) gives the buffer area, power and $P_{delay}$ results for the post processing technique detailed in section (2). The table also compares the results with those shown in Table (XXIII. The following inferences can be drawn from Table (XXIV). Post processing technique can be treated as a *fine tuning* technique and not an optimization procedure of its own. However, it does result in **3.8%** reduction in buffer area (and could be as high **9.9%**) on an average. Such a reduction though small could be significant in high performance designs. Post-processing does not have much of an impact on power dissipation and permissible delay.
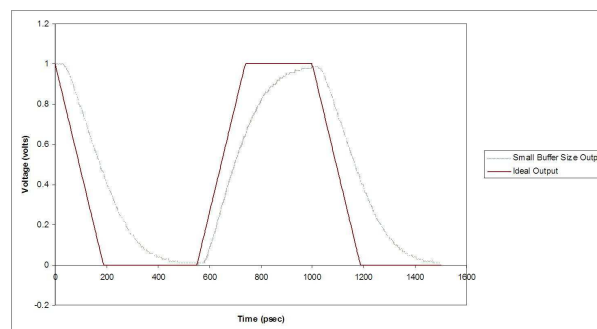


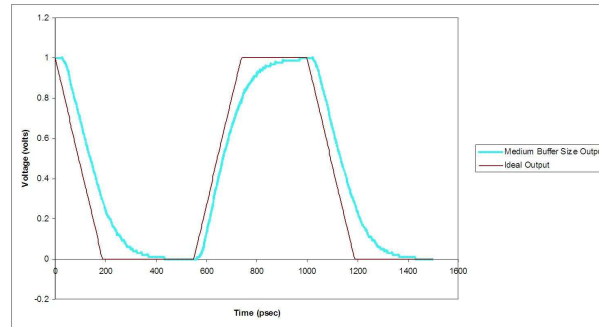Fig. 25. Worst case output waveform with small buffer size.

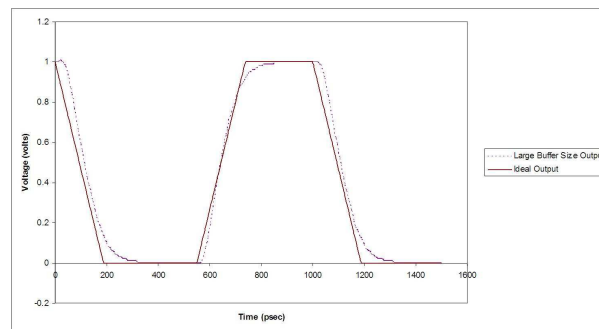Fig. 26. Worst case output waveform with medium buffer size.



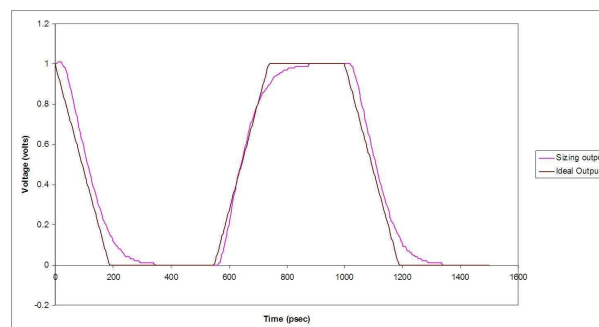Fig. 27. Worst case output waveform with large buffer size.



Fig. 28. Worst case output waveform with sizing algorithm.

Table XXIII. Results for mesh reduction.

| Case | Wire Length | | Pow | | $skew_{nom}$ | $\mu_{skew}$ | $\sigma_{skew}$ | $skew_{max}$ | $P_{delay}$ | |
|---|---|---|---|---|---|---|---|---|---|---|
| | $\mu m$ | % Imp. | mW | % Imp | (ps) | (ps) | (ps) | (ps) | (ps) | % Red |
| s9234 | 27177 | 10.5 | 6.7 | 6.1 | 33.0 | 45.4 | 7.8 | 68.7 | 931.3 | 1.3 |
| s5378 | 24911 | 22.9 | 6.7 | 14.0 | 29.1 | 44.7 | 6.4 | 63.8 | 936.2 | 0.3 |
| s13207 | 109538 | 28.6 | 23.8 | 21.5 | 22.9 | 60.0 | 22.5 | 127.5 | 872.5 | 3.3 |
| s15850 | 100778 | 38.8 | 23.8 | 28.1 | 21.8 | 37.5 | 11.3 | 71.2 | 928.8 | 1.0 |
| s38584 | 262528 | 29.4 | 60.9 | 22.0 | 33.0 | 70.5 | 16.0 | 118.5 | 881.5 | 0.9 |
| s35932 | 321293 | 24.9 | 74.3 | 19.6 | 36.2 | 71.2 | 12.3 | 108.1 | 891.9 | 0.9 |
| Ave | 131981 | 25.9 | 32.7 | 18.5 | 29.7 | 54.9 | 12.7 | 93.0 | 907.0 | 1.3 |

Power skew trade off
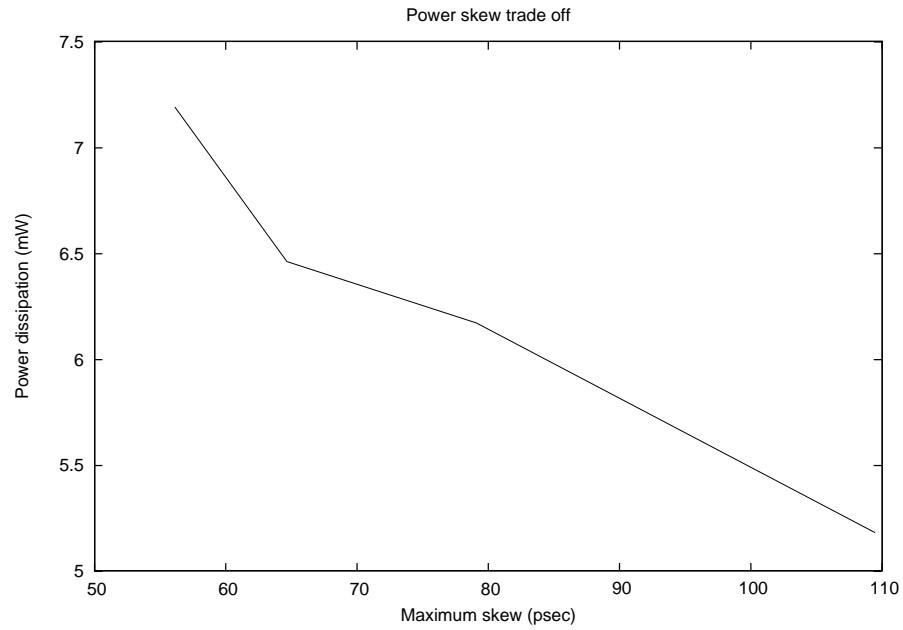
Fig. 29. Power vs. $skew_{max}$ trade off for s9234

Table XXIV. Reduction in buffer area and power after post-processing.

| Case | Buffer Area | Imp (%) | Pow | Imp(%) | $P_{delay}$ | Imp(%) |
|------|-------------|---------|-------|--------|-------------|--------|
| s9234 | 1100 | 3.5 | 7.35 | 0.68 | 931.3 | 0.0 |
| s5378 | 1350 | 0.0 | 7.42 | 0.00 | 936.1 | 0.0 |
| s13209 | 4740 | 2.7 | 24.48 | 0.41 | 872.5 | 0.0 |
| s15850 | 4840 | 9.9 | 23.98 | 2.12 | 928.8 | 0.0 |
| s38584 | 10880 | 4.7 | 63.20 | 0.88 | 881.5 | 0.0 |
| s35932 | 12660 | 1.8 | 78.51 | 0.24 | 891.9 | 0.0 |
| Ave | 5890 | 3.8 | 34.16 | 0.72 | 907.0 | 0.0 |

CHAPTER VI

CONCLUSIONS

We presented several techniques for two key problems in clock distribution networks: (a) Skew degradation due to PVT variations and (b) Power dissipation. Our techniques have been tested through extensive experimentation.

For tree based distributions, we integrated skew scheduling, topology generation and layout embedding into one framework - reduce maximum skew due to variations. In the proposed skew scheduling algorithm, process variations were considered directly in skew safety margin allocations so that a larger safety margin can be obtained for registers far apart. In the clock routing algorithm, a new layout embedding technique was developed to optimally minimize the maximum skew violation due to process variations. The effectiveness of the proposed algorithms was validated through Monte Carlo simulations on benchmark circuits. Experimental results indicate that our techniques can reduce the maximum skew violation by 19% on an average.

Link insertion has been shown to be an effective technique to reduce the clock skew due to variations with minimal increase in wire length. However, previous works on link insertion were restricted to unbuffered clock nets. In reality, buffers are needed to meet signal delay and slew constraints. We addressed the issues/risks involved in inserting links in buffered clock nets. A design criteria to avoid the short-circuit current was detailed. Link insertion works under the assumption that a low skew tree is available as input. We detail techniques to produce low skew trees under a higher order delay model. The tree generated is friendly towards link insertion. The effectiveness of link insertion was demonstrated via Monte Carlo simulations that considered all major source of variations. The simulations also took care of spatial correlations between the sources of variations. We compared our technique with both

tree and mesh (a popular form of non-tree based clock distribution). Experimental results indicate that our technique can be used to reduce the skew by over 32% with less than 5% increase in power dissipation.

Rotary clocking is a promising new clocking scheme that handles both power dissipation and skew variation simultaneously. We detailed the issues involved in adopting current CAD flow towards rotary clocking. Based on the problem specific constraints, we presented an alternative flow and algorithms. The proposed flow integrates clock skew optimization with placement. By utilizing intentional skew management and flip-flop clustering, both the phase and physical location constraints of the rotary clocking can be satisfied. We also proposed techniques to minimize the maximum load capacitance seen by the rotary rings. To the best of our knowledge, this is the first placement and skew optimization work for rotary clocking. Experimental results indicate that our techniques can reduce the tapping cost by 37%-52% with 2.6%-6% reduction in total wirelength. Since our method enables a concurrent clock network and placement design, it is potentially useful for other clocking methodologies like [62] as well. In our current methodology, we connect the ring directly to the flip-flops assigned to them. However, this could be improved by creating local trees that connect the ring location to a set of flip-flops. In such a construction, care should be taken to take care of the skew permissible ranges of the flip-flop pairs. Such a scheme could lead to potential benefits in wirelength and power dissipation. Further, our formulations take the number of rotary rings as part of the input. A better approach would be to integrate the number of rings as a variable in our methodology. This could lead to better optimization as it increases the solution space. We wish to investigate both these aspects in our future work.

Clock mesh is a very popular form of CDN among high performance systems. We addressed some key issues involved in the design and optimization of clock mesh.

We detailed a mesh buffer sizing/placement algorithms that places and sizes the mesh buffers in order to meet the signal slew constraints while minimizing the buffer cost. Clock mesh is tolerant towards variations in clock skew. The tolerance comes at the expense of redundancy created due to the multiple paths between the mesh buffers and the clock sinks. Such a redundancy also results in high power dissipation. We formulate the problem of mesh reduction by using concepts from survivable network theory. We remove selective number of mesh edges thereby trading off skew tolerance for lower power dissipation. The number of edges removed depends upon user defined parameters. Depending on these parameters the user can choose to remove large (implies low skew tolerance and low power) number of edges or small number of edges (implies high skew tolerance and high power). Our technique for mesh reduction is fast. Hence, the user can run the algorithm for different parameter values and choose the desired trade-off point. Our techniques indicate up to 28% reduction in power with less than 3.3% increase in maximum permissible delay.

REFERENCES

[1]  J. P. Fishburn, "Clock skew optimization", *IEEE Transactions on Computers*, vol. 39, no. 7, pp. 945–950, 1990.

[2]  Y. Liu, S. R. Nassif, L. T. Pileggi, and A. J. Strojwas, "Impact of interconnect variations on the clock skew of a gigahertz microprocessor", *IEEE/ACM Design Automation Conference*, pp. 168–171, 2000.

[3]  P. Saxena, N. Menezes, P. Cocchini and D. A. Kirkpatrick, "Repeater scaling and its impact on CAD", *IEEE Transactions Computer-Aided Design of Integrated Circuits and Systems*, vol. 23, no. 4, pp. 451–463, 2004.

[4]  R. Saleh, S. Z. Hussain, S. Rochel and D. Overhauser, "Clock skew verification in the presence of IR-drop in the power distribution network", *IEEE Transactions Computer-Aided Design of Integrated Circuits and Systems*, vol. 19, no. 6, pp. 635–644, 2000.

[5]  W. Liao and L. He, "Full-Chip interconnect power estimation and simulation considering concurrent repeater and flip-flop insertion", *IEEE/ACM International Conference on Computer-Aided Design*, pp. 574–580, 2003.

[6]  V. Tiwari, D. Singh, S. Rajagopal, G. Mehta, R. Patel and F. Baez, "Reducing power in high-performance microprocessors", *IEEE/ACM Design Automation Conference*, pp. 732–737, 1998.

[7]  C.-W. A. Tsao and C.-K. Koh, "UST/DME: a clock tree router for general skew constraints", *ACM Transactions on Design Automation of Electronic Systems*, vol. 7, no. 3, pp. 359–379, 2002.

[8] A. Rajaram, J. Hu, and R. Mahapatra, "Reducing clock skew variability via cross links", *IEEE/ACM Design Automation Conference*, pp. 18–23, 2004.

[9] A. Rajaram, D. Pan, and J. Hu, "Improved algorithms for link based non-tree clock network for skew variability reduction", *ACM International Symposium on Physical Design*, pp. 55–62, 2005.

[10] J. Wood, T. C. Edwards, and S. Lipa, "Rotary traveling-wave oscillator arrays: a new clock technology", *IEEE Journal of Solid-State Circuits*, vol. 36, no. 11, pp. 1654–1665, November 2001.

[11] G. Northrop, G. Averill, R. Barkley, K. Carey, S. Chan, et al., "609 MHz G5 S/399 microprocessor", *International Solid-State Circuits Conference*, pp. 88–89, 1999.

[12] P. J. Restle, C. A. Carter, J. P. Eckhardt, B. L. Krauter, B. D. McCredie, et al., "The clock distribution of the Power4 microprocessor", *International Solid-State Circuits Conference*, pp. 144–145, 2002.

[13] R. Heald. "Implementation of a 3rd-generation SPARC V9 64 b microprocessor", *International Solid-State Circuits Conference*, pp. 412–413, 2000.

[14] B. Lu, J. Hu, G. Ellis, and H. Su, "Process variation aware clock tree routing", *ACM International Symposium on Physical Design*, pp. 174–181, 2003.

[15] W. C. Elmore, "The transient analysis of damped linear networks with particular regard to wideband amplifiers", *Journal of Applied Physics*, vol. 19, no. 1, pp. 55–63, 1948.

[16] J. Rubinstein, P. Penfield, and M. A. Horowitz, "Signal delay in RC tree networks", *IEEE Transactions on Computer-Aided Design of Integrated Circuits*

*and Systems*, CAD vol. 2, no. 3, pp. 202–211, July 1983.

[17] T.-H. Chao, Y.-C. Hsu, J.-M.Ho, K. D. Boese and A. B. Kahng, "Zero skew clock routing with minimum wirelength", *IEEE Transactions on Circuits and Systems-II*, vol. 39, no. 39, pp. 799–814, 1992.

[18] R. S. Tsay. "An exact zero-skew clock routing algorithm", *IEEE Transactions Computer-Aided Design of Integrated Circuits and Systems*, vol. 12, no. 2, pp. 242–249, 1993.

[19] R. B. Deokar and S. S. Sapatnekar, "A graph-theoretic approach to clock skew optimization", *International Symposium of Circuits and Systems*, pp. 407–410, 1994.

[20] M. Edahiro, "A clustering-based optimization algorithm in zero-skew routings", *IEEE/ACM Design Automation Conference*, pp. 612–616, 1993.

[21] D. Velenis, M. C. Papaefthymiou, and E. G. Friedman, "Reduced delay uncertainty in high performance clock distribution networks", *Design Automation and Test Europe*, pp. 68–73, 2003.

[22] R. Chaturvedi and J. Hu, "A simple yet effective merging scheme for prescribed-skew clock routing", *International Conference on Computer Design*, pp. 282-287, 2003.

[23] C. Albrecht, B. Korte, J. Schietke, and J. Vygen, "Cycle time and slack optimization for VLSI-chips", *IEEE/ACM International Conference on Computer-Aided Design*, pp. 232–238, 1999.

[24] I. S. Kourtev and E. G. Friedman, "Clock skew scheduling for improved reliability via quadratic programming", *IEEE/ACM International Conference on*

*Computer-Aided Design*, pp. 239–243, 1999.

[25] N. Bindal, T. Kelly, N. Velastegui, and K. L. Wong, "Scalable sub-10ps skew global clock distribution for a 90nm multi-GHz IA microprocessor", *IEEE International Solid-State Circuits Conference*, pp. 346–355, 2003.

[26] S. Zanella, A. Nardi, A. Neviani, M. Quarantelli, S. Saxena, and C. Guardiani, "Analysis of the impact of process variations on clock skew", *IEEE Transactions on Semiconductor Manufacturing*, vol. 13, no. 4, pp. 401–407, November 2000.

[27] R. Saleh, S. Z. Hussain, S. Rochel, and D. Overhauser, "Clock skew verification in the presence of IR-drop in the power distribution network", *IEEE Transactions on Computer-Aided Design*, vol. 19, no. 6, pp. 635–644, June 2000.

[28] C. Visweswariah, "Death, taxes and failing chips", *IEEE/ACM Design Automation Conference*, pp. 343–347, 2003.

[29] H. Chang and S. S. Sapatnekar, "Statistical timing analysis considering spatial correlations using a single PERT-like traversal", *IEEE/ACM Int Conference on Computer Aided Design* , pp. 621–625, 2003.

[30] A. Rajaram, D. Z. Pan, "Variation tolerant buffered clock network synthesis with cross links", *ACM International Symposium oh Physical Design*, pp. 157–164, 2006.

[31] G. Venkataraman, N. Jayakumar, J. Hu, P. Li, S. Khatri, A. Rajaram, P. McGuinness and C. Alpert, "Practical techniques to reduce skew and its variations in buffered clock networks", *IEEE/ACM International Conference on Computer Aided Design*, pp. 592–596, 2005.

[32] J. Wyatt, "Signal delay in RC mesh networks", *IEEE Transactions on Computer-Aided Design*, vol. 32, no. 5, pp. 507–510, May 2005.

[33] J. L. Tsai, D. Baik, C. C. Chen and K. Saluja, "A yield improvement methodology using pre- and post-silicon statistical clock scheduling", *IEEE/ACM International Conference on Computer Aided Design*, pp. 611–618, 2004.

[34] S. Pullela, N. Menezes, J. Omar, and L. T. Pillage, "Skew and delay optimization for reliable buffered clock trees", *IEEE/ACM International Conference on Computer-Aided Design*, pp. 556–562, 1993.

[35] J. G. Xi and W. W.-M. Dai, "Buffer insertion and sizing under process variations for low power clock distribution", *IEEE/ACM Design Automation Conference*, pp. 491–496, 1995.

[36] X. Zeng, D. Zhou, and W. Li, "Buffer insertion for clock delay and skew minimization", *ACM International Symposium on Physical Design*, pp. 36–41, 1999.

[37] R. Chaturvedi and J. Hu, "Buffered clock tree for high quality IC design", *IEEE International Symposium on Quality Electronic Design*, pp. 381–386, 2004.

[38] K. Wang and M. Marek-Sadowska, "Clock network sizing via sequential linear programming with time-domain analysis", *ACM International Symposium on Physical Design*, pp. 182–189, 2004.

[39] A. B. Kahng and B. Liu. "Q-Tree: A new iterative improvement approach for buffered interconnect optimization", *IEEE Comp. Soc. Annual Symp. On VLSI*, pp. 183-188, February, 2003.

[40] Y. Cao. "Predictive Technology Model", Nanoscale integration and modeling group, Arizona State Univerity, Downloaded on April 2, 2006 from

http://www.eas.asu.edu/~ptm/.

[41] E. M. Sentovich, K. J. Singh, L. Lavagno, C. Moon, R. Murgai, A. Saldanha, H. Savoj, P. R. Stephan, R. K. Brayton, and A. L. Sangiovanni-Vincentelli, "SIS: a system for sequential circuit synthesis", Memorandum no. M92/41, ERL, University of California, Berkeley, May 1992.

[42] "CPMO-constrained placement by multilevel optimization", Computer Science Department, UCLA, Downloaded on March 1, 2005 from http://cadlab.cs.ucla.edu/cpmo/mpl.

[43] R. O'Mahony, C. P. Yue, M. A. Horowitz, and S. S. Wong, "A 10-GHz global clock distribution using coupled standing-wave oscillators", *IEEE Journal of Solid-State Circuits*, vol. 38, no. 11, pp. 1813–1820, November 2003.

[44] S. C. Chan, K. L. Shepard, and P. J. Restle, "Uniform-phase uniform-amplitude resonant-load global clock distributions", *IEEE Journal of Solid-State Circuits*, vol. 40, no. 1, pp. 102–109, January 2005.

[45] Z. Yu and X. Liu, "Power analysis of rotary clock", *IEEE Computer Society Annual Symposium on VLSI*, pp. 150–155, 2005.

[46] S. Held, B. Korte, J. Maβberg, M. Ringe, and J. Vygen, "Clock scheduling and clock tree construction for high performance ASICs", *IEEE/ACM International Conference on Computer-Aided Design*, pp. 232–239, 2003.

[47] H. Eisenmann and F. M. Johannes, "Generic global placement and floorplanning", *IEEE/ACM Design Automation Conference*, pp. 269–274, 1998.

[48] T. F. Chan, J. Cong, J. Shinnerl, and K. Sze, "An enhanced multilevel algorithm

for circuit placement", *IEEE/ACM International Conference on Computer-Aided Design*, pp. 299–306, 2003.

[49] R. K. Ahuja, T. L. Magnanti, and J. B. Orlin, *Network Flows: Theory, Algorithms, and Applications.* Upper Saddle River, NJ:Prentice Hall, 1993.

[50] P. J. Restle, T. G. McNamara, D. A. Webber, P. J. Camporese, K. F. Eng, K. A. Jenkins, D. H. Allen, M. J. Rohn, M. P. Quaranta, D. W. Boerstler, C. J. Alpert, C. A. Carter, R. N. Bailey, J. G. Petrovick, B. L. Krauter, and B. D. McCredie, "A clock distribution network for microprocessors", *IEEE Journal of Solid-State Circuits*, vol. 36, no. 5, pp. 792–799, May 2001.

[51] V. V. Vazirani, *Approximation Algorithms*, New York:Springer 2001.

[52] "GNU linear programming kit", Downloaded on December 15, 2005 from http://www.gnu.org/software/glpk/glpk.html.

[53] R. Wunderling, "Paralleler und Objektorientierter Simplex-Algorithmus", ZIB Technical Report TR 96-09, Berlin, 1996.

[54] C. J. Alpert, J. Hu, S. S. Sapatnekar and C. N. Sze, "Accurate estimation of global buffer delay within a floorplan", *IEEE Transactions on Computer-Aided Design*, vol. 25, no. 6, pp. 1140–1145, June 2006.

[55] N. A. Kurd, J. S. Barkatullah, R. O. Dizon, T. D. Fletcher, and P. D. Madland, "A multigigahertz clocking scheme for the Pentium 4 microprocessor", *IEEE Journal of Solid-State Circuits*, vol. 36, no. 11, pp. 1647–1653, November 2001.

[56] H. Su and S. Sapatnekar, "Hybrid structured clock network construction", *International Conference on Computer-Aided Design*, pp., 333–336, 2001.

[57] M. Donno, Enrico Macii and L. Mazzoni, "Power aware clock tree planning", *ACM International Symposium on Physical Design*, pp. 138–147, 2004.

[58] U. Feige, "A threshold of ln(n) for approximating set cover", *Journal of ACM*, vol. 45, no. 4, pp. 634–652, 1998.

[59] K. Jain, "A factor 2 approximation algorithm for the generalized steiner network problem", *IEEE Symposium on Foundations of Computer Science*, pp. 448–457, 1998.

[60] H. Kerivin and A. R. Mahjoub, "Design of survivable networks: A survey", *Networks*, vol. 46, no. 1, pp. 1–21, April 2005.

[61] W Ben-Ameur, "Constrained length connectivity and survivable networks", *Networks*, vol. 36, no. 1, pp. 17–23, August 2000.

[62] Y. Lu, C. N. Sze, X. Hong, Q. Zhou, Y. Cai, L. Huang, and J. Hu, "Navigating registers in placement for clock network minimization", *IEEE/ACM Design Automation Conference*, pp. 176–181, 2005.

VITA

Ganesh Venkataraman received his B. E. (Hons) Electrical and Electronics and M. Sc. (Hons) Physics from the Birla Institute of Technology and Science, Pilani, India in 2000. He completed his M. S. in Electrical and Computer Engineering from the University of Iowa in the year 2003.

Ganesh worked as Design Engineer at Cypress Semiconductor between June 2000 and June 2001. He worked as a summer intern at Intel (summer 2005) and IBM Austin Research Lab (2006).

His research interests include VLSI physical design, variation tolerant clock distributions, low power, placement, routing, gate sizing, graph theory and combinatorial optimization. His works have been published in leading international conferences including International Conference of Computer-Aided Design (ICCAD), Asia and South Pacific Design Automation Conference (ASPDAC), Design Automation and Test Europe (DATE) and Symposium on Discrete Algorithms (SODA).

Ganesh received the Graduate Merit Fellowship from Texas A&M University. This fellowship is awarded via university wide competition among incoming graduate students. He received the Government Merit Scholarship in the year 1993 and 1995. This is awarded by the Government of India to the 0.1% of the 100,000+ students who took the $10^{th}$ and $12^{th}$ standard CBSE examinations in the year 1993 and 1995 respectively. He was the President of the Association for India's Development (AID) TAMU chapter in the year 2005-06.

Ganesh can be reached at the Department of Electrical and Computer Engineering, 333 WERC, Texas A&M University, TX - 77843.

The typist for this dissertation was Ganesh Venkataraman.